Differential regulation of mouse hippocampal gene expression sex differences by chromosomal content and gonadal sex

Authors: Sarah R. Ocañas[1,2], Victor A. Ansere[1,2], Kyla B. Tooley[1,2], Niran Hadad[2], Ana J. Chucair-Elliott[1], David R. Stanford[1], Shannon Rice[1], Benjamin Wronowski[2], Jessica M. Hoffman[3], Steven N. Austad[3], Michael B. Stout[4], Willard M. Freeman[1,5*]

[1]Genes & Human Disease Program, Oklahoma Medical Research Foundation, Oklahoma City, OK USA, [2]Department of Physiology, University of Oklahoma Health Sciences Center, Oklahoma City, OK USA, [3]Department of Biology, The University of Alabama at Birmingham, Birmingham, AL USA, [4]Aging & Metabolism Disease Program, Oklahoma Medical Research Foundation, Oklahoma City, OK USA, [5]Oklahoma City Veterans Affairs Medical Center, Oklahoma City, OK USA

To whom correspondence should be addressed: [*]Willard M. Freeman, Genes & Human Disease Program, Oklahoma Medical Research Foundation, 825 NE 13th Street, Oklahoma City, OK 73104, USA.

Tel: 405-271-3139

Fax: 405-271-2536

E-mail address: bill-freeman@omrf.org

Acknowledgments: This work was supported by grants from the National Institutes of Health (NIH) P30AG050911, R01AG059430, R56AG067754, T32AG052363, F31AG064861, P30EY021725, P30AG050886, R21AG058811, R01AG057434, R01AG070035, R01AG069742, Oklahoma Center for Adult Stem Cell Research (OCASCR), a program of the Oklahoma Tobacco Settlement Endowment Trust, BrightFocus Foundation (M2020207), and Presbyterian Health Foundation. This work was also supported in part by the MERIT award I01BX003906 and a Shared Equipment Evaluation Program (ShEEP) award ISIBX004797 from the United States (U.S.) Department of Veterans Affairs, Biomedical Laboratory Research and Development Service. The authors would also like to thank the Clinical Genomics Center (OMRF) for assistance and instrument usage.

Abstract

Sex differences in the brain as they relate to health and disease are often overlooked in experimental models. Many neurological disorders, like Alzheimer's disease (AD), multiple sclerosis (MS), and autism, differ in prevalence between males and females. Sex differences originate either from differential gene expression on sex chromosomes or from hormonal differences, either directly or indirectly. To disentangle the relative contributions of genetic sex (XX v. XY) and gonadal sex (ovaries v. testes) to the regulation of hippocampal sex effects, we use the "sex-reversal" Four Core Genotype (FCG) mouse model which uncouples sex chromosome complement from gonadal sex. Transcriptomic and epigenomic analyses of hippocampal RNA and DNA from ~12 month old FCG mice, reveals differential regulatory effects of sex chromosome content and gonadal sex on X- versus autosome-encoded gene expression and DNA modification patterns. Gene expression and DNA methylation patterns on the X chromosome were driven primarily by sex chromosome content, not gonadal sex. The majority of DNA methylation changes involved hypermethylation in the XX genotypes (as compared to XY) in the CpG context, with the largest differences in CpG islands, promoters, and CTCF binding sites. Autosomal gene expression and DNA modifications demonstrated regulation by sex chromosome complement and gonadal sex. These data demonstrate the importance of sex chromosomes themselves, independent of hormonal status, in regulating hippocampal sex effects. Future studies will need to further interrogate specific CNS cell types, identify the mechanisms by which sex chromosome regulate autosomes, and differentiate organizational from activational hormonal effects.

Keywords

Sex effects, hippocampus, epigenome, transcriptome, four core genotype, sex chromosome, DNA methylation, X inactivation

Introduction

Sex is a major risk factor for many neurological diseases and disorders, including Alzheimer's disease (AD), multiple sclerosis, autism, attention-deficit/hyperactivity disorder (ADHD), depression, and age-related cognitive decline. Females tend to outperform males on hippocampal-dependent learning tasks and are more impacted by many diseases/disorders of hippocampal dysfunction (i.e. AD, depression)[1]. As the learning center of the brain, damage to the hippocampus leads to cognitive decline. Understanding basal sex differences and their regulation in the hippocampus can help gain insight into the etiology of sex differences in hippocampal dysfunction in common neurological diseases. The focus of this study is to understand the regulation of hippocampal transcriptomic and epigenomic sex differences as they are affected by gonadal sex and/or sex chromosomal content.

At the most basic level, sex determination in mammals occurs as a result of sex chromosome complement. The presence or absence of the sex-determining region of Y (*Sry*) gene, encoded on the Y chromosome, is necessary and sufficient for development of testis. In the absence of *Sry,* mammals develop ovaries. As such, development into a gonadal female generally occurs when the embryo has two X and no Y chromosomes, whereas a gonadal male develops when the embryo has one copy of X and one copy of Y chromosome.

After gonad differentiation into testis or ovaries, hormonal secretions influence the organism's sexual phenotype. There are organizational effects of hormonal secretions that cause irreversible sex differentiation and activational effects may be temporary and reversible and can occur at any stage of life[2]. In a seminal paper, Phoenix et al (1959)[3] described the organizational-activational theory of sexual differentiation in which during early development, hormones have an organizational effect on neural tissue development and circuitry that mediates mating (and likely other behaviors). During adulthood, once the organizational framework is established, activational effects are mediated in the presence of gonads and related sex hormones. Gonadectomies with and without hormone replacement can be used in animal models to study the activational effects of gonadal hormones. For example, gonadectomized rats showed a memory deficit in Morris water maze testing, along with a decrease in androgen receptor-immunoreactive neurons. Treatment with testosterone in the gonadectomized rats attenuated the cognitive deficits and increased the number of androgen receptor-immunoreactive neurons[4]. Postnatal gonadectomies and/or hormone therapies have been used to separate activational and organizational contributions of sex hormones on phenotypic sex differences in the hippocampus in both rats[5-7]

and mice[8-10] with mixed results regarding phenotypic effects. As such, both gonadal hormones and sex chromosome complement likely contribute to sex effects in the hippocampus.

In summary, the direct contributors to phenotypic sex effects are: (1) activational effects of sex hormones, (2) organizational effects of sex hormones, and (3) sex chromosome effects[11]. There is an inherent difficulty in studying relative contributions of the three causes of sex effects, since the gonadal/hormonal sex and chromosomal sex are naturally coupled.

However, understanding these relative contributions of hormones and chromosomal content to health and disease is a public health imperative. For example, activational effects of hormones are an attractive target for therapeutic interventions (i.e., hormone replacement therapy (HRT)) in neurological conditions with sex differences. Nevertheless, this approach has been met with variable success. Observational studies of HRT effects on cognitive function in AD and Mild Cognitive Impairment (MCI) have had mixed results. A randomized, double-blind, placebo-controlled clinical trial was conducted to determine if administration of estrogen replacement therapy had an effect on cognition in women with AD that had received a hysterectomy showed no effect on the progression of cognitive decline after one year [12].

Despite being the biggest genomic difference between humans, the role of sex chromosomes in sex effects is complex and still mostly unclear. The Y chromosome only contains around 70 protein-coding genes, it also encodes more than 100 noncoding RNAs of unknown function. Moreover, the mosaic loss of Y chromosome with age has been linked to several cancers as well as Alzheimer's disease. The X chromosome is relatively gene dense with between 900 and 1500 genes, but its expression profile is complicated by the random inactivation of one X-chromosome on a cell-by-cell basis due to dosage compensation[13]. Sex chromosome aneuploidies seen in humans include Turner syndrome (XO), Triple X Syndrome (XXX), and Kleinfelter syndrome (XXY). Females with Turner syndrome, or X monosomy, are generally shorter in stature, have gonadal dysfunction, and are at a greater risk for autoimmune diseases and learning disabilities, such as autism, ADHD, and other neurodevelopment disorders[14]. Females with Triple X syndrome, or Trisomy X, have widely variable symptoms that can include delayed speech and language skills, learning disabilities, increased prevalence of ADHD/autism, and increased anxiety and depression. Males with Klinefelter syndrome have more anxiety/depression, ADHD, and autism, as well as developing autoimmune diseases at higher rates more similar to XX females [15]. From these naturally occurring chromosome anomalies in humans, it appears that sex chromosome complement, especially the number of X chromosomes, could also play a role in sex differences seen in common neurological conditions.

Sex chromosome complement (XX vs. XY) can affect brain development through a variety of mechanisms: 1) The presence or absence of *Sry* (and other Y encoded genes), 2) X chromosome inactivation through *Xist*, 3) Dosage of X chromosome genes (1X vs 2X) and X chromosome imprinting, 4) Epigenetics (DNA modifications, chromatin accessibility, histone modifications, etc) of the sex chromosomes (X and Y), and 5) autosomal epigenetics due to a sex chromosome encoded factor[16]. In addition, with aging epigenetic changes such as loss of silencing, progressively increasing bias in paternal vs maternal X-inactivation, and even mosaic loss of the Y-chromosome all may contribute to sex differences in neurodegenerative processes and other aspects of health.

Of particular interest in epigenetic factors is methylation - the fifth carbon of cytosine, resulting in DNA modification 5-methyl-cytosine (mC). This modification is generally studied in the context of CpG dinucleotides due to their palindromic representation across DNA strands allowing for fidelity in maintaining modification patterns in mitotic cells. Neurons and other post-mitotic cells in the brain show higher levels of non-CpG (CH) methylation than other non-CNS tissue.

X-chromosome inactivation (XCI) is a mechanism that causes silencing of a random X-chromosome during female embryogenesis and XCI is an important mechanism in X-chromosome gene dosage compensation between males and females[17]. Maintenance of XCI in somatic cells occurs via a combination of epigenomic mechanisms, including DNA methylation. LncRNA *Xist* coats the inactive X-chromosome (Xi) and recruits chromatin modifiers to stably repress transcription from Xi. Hallmarks of XCI include changes to histone modifications and hypermethylation of cytosine residues in CG contexts[18]. However, Xi is not fully repressed and a subset of X-chromosome genes are consistently expressed from the Xi, leading to higher overall gene expression in females[19,20]. Further, escape from X-inactivation in females has been implicated in the female bias in autoimmune diseases[21,22] and Alzheimer's disease[23].

Previous reports have established sex differences in the hippocampal epigenome and transcriptome with brain aging[24,25] and disease[26-28]. To disentangle the effects of sex (testes v. ovaries; M v. F) and sex chromosome complement (XX v. XY) on the steady state gene expression and DNA modification patterning of the hippocampus, we use the Four Core Genotype (FCG) mouse model[29]. The FCG model involves a translocation of the *Sry* from the Y chromosome to an autosome on a C57BL/6 background, resulting in the FCG XY male (XYM). Crossing the XYM with a wildtype XX female (XXF), results in the FCG: XX and XY mice with testes (XXM/XYM) and XX and XY mice with ovaries (XXF/XYF) (**Figure 1A**). This allows for 2-

153 way statistical comparisons to assess the hormonal, chromosomal, and interactive effects on
154 molecular and phenotypic outcomes.

155 Early FCG mouse studies were aimed at determining if sex chromosome complement (XX v. XY)
156 played an important role in development of well-established sexually dimorphic phenotypes. Male
157 copulatory behavior, social exploration behavior, and anatomical organization of the central
158 nervous system were found to be regulated primarily by gonadal hormones regardless of sex
159 chromosome complement[30-33]. In addition to sex hormone effects on brain development, FCG
160 studies have shown sex chromosome complement influences neuronal phenotype[34],
161 nociception[35], and neural tube closure[36]. Using FCG model in combination with Experimental
162 Autoimmune Encephalomyelitis (EAE) and pristane-induced Systemic Lupus Erythematosus
163 (SLE) models shows a sex chromosome effect (XX v. XY) on disease severity with worse disease
164 scores in XX genotypes as compared to XY phenotypes, regardless of gonadal sex (M v. F)[37].
165 Additionally, the XX mice have longer lifespans, regardless of gonadal sex[38], and XX mice have
166 resiliency to death in an AD mouse model[39].

167 Although hippocampal sex differences in the transcriptome and epigenome are well-established
168 across development, aging, and disease in mice and humans, the relative contributions of sex
169 chromosome complement (XX v. XY) and gonadal sex (M v. F) to the steady state and stimulus
170 responsive transcriptome and epigenome are not fully defined.

171 In this study, we use transcriptomic and epigenetic approaches to examine the hippocampal
172 transcriptome and methylome in adult FCG mice. We then compare our findings to previously
173 identified hippocampal sex differences (both in normal conditions and in disease) to begin to
174 disentangle contributions of sex chromosome complement (XX v. XY) and gonadal sex (testes v.
175 ovaries; M v. F) to sex differences in transcriptional programming.

176 **Results**

177 ***Sry* copy number and localization in adult FCG hippocampi.**

178 The testis-determining *Sry* gene is considered the “master switch” in mammalian sex
179 determination. During mammalian embryogenesis, bipotential gonads form from the genital ridge
180 with a default to become ovaries. Expression of *Sry* upregulates SRY box containing gene 9
181 (*Sox9*) which leads to the differentiation of Sertoli cells, the formation of testis, and the
182 suppression of the female sex-determining pathway[40]. In the FCG model, *Sry* is deleted from the
183 Y chromosome and *Sry* is translocated onto an autosome, uncoupling gonadal sex from genetic

sex. The localization of Sry however has not been fully determined. Previous initial reports[41] used fluorescence *in situ* hybridization (FISH) to localize a concatemer of *Sry* on chromosome 3 in FCG males. We sought to determine the number of copies of the *Sry* gene and to precisely mark the location of the translocated *Sry* as well as if there was more than one site of translocation. A novel digital PCR *Sry* copy number assay performed on FCG hippocampal DNA confirmed 12-14 copies of *Sry* in FCG males (XXM/XYM), as compared to one copy in WT males (**Figure 1B**). Linked read sequencing of high molecular weight DNA from FCG XYM shows no linkage between *Sry* gene and the adjacent region of the Y chromosome (**Figure 1C**) and strong linkage of *Sry* with a region on chromosome 3 (**Figure 1D**) within a region with no known gene annotation.

Transcriptomic analysis of sex chromosomal (X/Y) differential expression from adult FCG hippocampi.

After quantifying and localizing *Sry* we sought to determine the relative contributions of gonadal and sex chromosomal content to transcriptomic regulation of the sex chromosomes (X/Y) through RT-qPCR and RNA-Seq analyses.

In mammals, females have two X chromosomes and males only have one X chromosome. This results in a difference in X chromosome gene dosage requiring compensatory mechanisms to balance X chromosome gene expression in both sexes. Compensation for double dosage of X chromosomes in females can occur by: decreasing (halving) female X chromosome gene expression through inactivation of one X chromosome copy, or increasing (doubling) male X chromosome gene expression, or a combination of these two mechanisms.

Despite compensatory mechanisms, there are a number of X chromosome genes whose expression is imbalanced between males and females in the mouse hippocampus. Previous reports have established differentially expressed sex chromosomally-encoded genes in the mouse hippocampus throughout development and aging[26,42-44] (**Supplemental Table 1; GEO Accession:** GSE83931, GSE135752, GSE76567**; SRA bioProject:** PRJNA523985). Intersection of sex chromosomally-encoded (X/Y) differentially expressed genes by sex, identified eight common genes across all studies (**Figure 2A, Supplemental Table 1**), including X chromosome genes (*Xist, Ddx3x, Kdm6a,* and *Eif2s3x*) and Y chromosome genes (*Kdm5d, Eif2s3y, Uty, Ddx3y*). The four common ChrX genes (*Xist, Ddx3x, Kdm6a,* and *Eif2s3x*) have all been identified as genes likely to escape X-inactivation[45]. The Xi escape of *Ddx3x*, *Kdma6a*, and *Eif2s3x* are likely due to intolerance of haploinsufficiency, as each of these genes have Y-encoded paralogs *Ddx3y, Uty, and Eif2s3y*, respectively. Mutations in *Ddx3x*, *Kdma6a*, and *Eif2s3x* have

all been associated with X-linked intellectual disability[46,47]. Differences in the functionality of the X- and Y-encoded paralogues may contribute to sex-biases observed in brain disease. For example, although X-encoded *Kdm6a* has histone demethylase activity, the Y-encoded parolog *Uty* is catalytically inactive[48]. A recent study showed that a second X chromosome conferred resilience in a mouse model of AD, independent of gonadal sex, in part due to the 'double-dose' of *Kdm6a*[48].

We first wanted to establish that dosage compensatory gene *Xist* was induced by sex chromosome complement (XX v. XY) in FCG hippocampi, regardless of gonadal sex (M v. F).

X-inactive specific transcript (*Xist*) is a non-coding RNA that stabilizes the inactive X chromosome (Xi) and interacts with various silencing factors to alter chromatin accessibility through a variety of epigenetic mechanisms[49]. RNA isolated from FCG (XXF, XYF, XXM, XYM) hippocampi (n=10-16/group) was assessed for *Xist* expression by RT-qPCR. In the FCG hippocampus, *Xist* was differentially expressed by sex chromosome complement (XX v. XY) regardless of gonadal sex, with no detected expression in XY genotypes (**Figure 2B**; Two-way ANOVA, Main effect of sex-chromosome complement (XX v. XY), ***$p<0.001$) and no effect of gonadal sex. Sex differences in *Xist* expression in the FCG hippocampus parallels that of wild type animals and shows a clear influence of sex chromosome complement in the modulation of X-chromosome dosage compensation.

Lysine demethylase 5D (*Kdm5d*) is a Y-chromosome encoded gene that mediates H3K4 demethylation and has been shown to be important in modulating sexually dimorphic gene expression[50]. DEAD-Box Helicase 3 Y-Linked (*Ddx3y*) is part of the male-specific region of the Y chromosome and contains a conserved Asp-Glu-Ala-Asp (DEAD) motif that are used by ATP-dependent RNA helicases[51]. Expression of Y-chromosome genes *Kdm5d* and *Ddx3y* were assessed by RT-qPCR. In the FCG hippocampus, there was a main effect of chromosome (XX v. XY) on *Kdm5d* and *Ddx3y* expression, with higher expression in XY and no detected expression in XX genotypes (**Figure 2C-D**; Two-way ANOVA, main effect of sex-chromosome complement (XX v. XY), ***$p<0.001$). There was no main effect of gonadal sex (M v. F) on the expression of *Kdm5d* or *Ddx3y* in the FCG hippocampus.

To assess the transcriptome in an unbiased manner, Directional RNA Sequencing (RNA-Seq) libraries were prepared from FCG hippocampal RNA (n=5-6/group) and sequenced on Illumina's NextSeq500 platform. After aligning, quantifying, and calling differentially expressed genes in StrandNGS software, twenty differentially expressed X-chromosome genes were identified with a

main effect of chromosome (XX v. XY) regardless of sex (M v. F) with nine genes higher and 11 genes lower in XX vs. XY (**Figure 2E**; Two-Way ANOVA, BHMTC, FC>=1.25, FDR<0.1). Among these genes were the eight previously identified genes from **Figure 2A**. Only two X chromosome genes (*Ace2, Aff2*) were differentially expressed by sex (M v. F) (**Figure 2F-G**; Two-Way ANOVA, BHMTC, FC>=1.25, FDR<0.1).

Four Y-encoded genes were found to be expressed and each of the four Y chromosome genes were differentially expressed by chromosome (XX v. XY) (**Figure 2H**; Two-Way ANOVA, BHMTC, FC>=1.25, FDR<0.1). There were no Y chromosome genes differentially expressed by sex (M v. F).

Erythroid differentiation regulator 1 (*Erdr1*) is part of X and Y chromosome pseudoautosomal region (PAR) that is able to crossover and recombine during meiosis. As such, genes within the PAR have the same sequence on the X and Y chromosome and the chromosomal origin (X or Y) of these transcripts cannot be determined with traditional RNA-Seq. In FCG hippocampi, *Erdr1* is differentially expressed by sex chromosome complement (XX v. XY), with higher levels in XX animals (**Figure 2I**).

The eight common previously identified X/Y-chromosome sex differences (**Figure 2A, Supplemental Table 1 (Intersection)**) were all differentially expressed by sex chromosome complement (XX v. XY) but not gonadal sex in the adult FCG hippocampus. When comparing the union of all sex differentially expressed genes from previous hippocampal studies (**Figure 2A, Supplemental Table 1 (Union)**) to the differentially expressed genes by sex chromosome complement (XX vs. XY) in the FCG hippocampus (**Figure 2B-I**) there are 18 genes in common (**Figure 2J**). After running these 18 genes through the Gene Ontology (GO), four biological processes were overrepresented (Fisher's Exact, FDR<0.05), including: 1) positive regulation of translational fidelity, 2) histone H3-K27 demethylation, 3) histone H3-K4 demethylation, and 4) formation of translation preinitiation complex (**Figure 2K**). Regulation of histone H3-K27 and H3-K4 methylation have both been implicated in the initiation and maintenance of X-chromosome inactivation[52].

Sex chromosome (X/Y) methylation patterns by Whole Genome Oxidative Bisulfite Sequencing (WGoxBS) in FCG hippocampi.

DNA methylation can regulate gene expression by a variety of mechanisms, including (but not limited to): 1) direct transcription inhibition by blocking transcription factor binding[53], 2) indirect transcription regulation by recruitment of chromatin modifiers and methyl binding proteins[54-57], 3)

genomic imprinting[58], and 4) X-chromosome inactivation[59-61]. Although methylated DNA is generally associated with transcriptional silencing, there are reported cased where DNA methylation may also serve an activational role[62].

In females, X-chromosome inactivation (XCI) occurs through multi-layer epigenetic mechanisms that ultimately compact the inactive X-chromosome (Xi) into a heterochromatic Barr Body. Early in development, the long-noncoding RNA (lncRNA) *Xist* is expressed from Xi and provides a *cis*-coating that recruits protein complexes, leading to changes in chromatin accessibility and DNA modifications[13]. Changes in histone modifications[52] and DNA methylation stabilizes Xi in the inactive state[63]. In this study, we assess the efficacy of Xi epigenetic silencing in the FCG mouse model by analyzing the X chromosome DNA methylation patterning in FCG hippocampal DNA.

To assay DNA methylation, DNA isolated from FCG hippocampi (n=3/group) was oxidized and bisulfite-converted prior to constructing whole genome libraries for sequencing on Illumina's NovaSeq6000 platform. After aligning and calling methylation values, the whole genome methylation levels in both CG and non-CG (CH) contexts were calculated. There were no observed differences in overall whole genome methylation in CG context (mCG) (**Figure 3A**) by sex (M v. F) or sex chromosome complement (XX v. XY).

When focused on the X chromosome, XX genotypes have higher mCG levels than XY genotypes, regardless of sex (M v. F) (**Figure 3B**; Two-way ANOVA, main effect sex chromosome complement (XX v. XY), ***p<0.001). There was no difference in mCG percentages in repetitive elements on the X-chromosome (**Figure 3C**; Two-way ANOVA) but in non-repetitive elements, higher methylation in XX genotypes than XY genotypes regardless of their gonadal sex was observed (**Figure 3D**; Two-way ANOVA, main effect sex chromosome complement (XX v. XY), ***p<0.001). In non-CpG (CH) context, there was no overall difference in methylation (**Figure 3E**). However, there was higher X-chromosome mCH in XY than XX, regardless of gonadal sex (**Figure3F;** Two-way ANOVA, main effect sex chromosome complement (XX v. XY), ***p<0.001). Higher XY mCH was seen in both repetitive (**Figure 2G**) and non-repetitive (**Figure 3H**) elements of the X-chromosome, as compared to XX (Two-way ANOVA, main effect sex chromosome complement (XX v. XY), ***p<0.001). These X-chromosomal methylations trends are consistent with previous reports[64].

Since the sex chromosome complement (XX v. XY) difference in mCG appears to be concentrated in non-repetitive elements of the X chromosome, we assessed the mCG patterning in and around CpG islands, gene bodies, and CTCF binding sites. CpG islands (CGIs) are

relatively long stretches (500-2000nt) of GC-rich DNA that are predominantly unmethylated[65]. CGIs have higher methylation on the Xi[66]. In the FCG hippocampi, XX genotypes have higher mCG within CGIs, shores, and shelves than XY genotypes, regardless of gonadal sex. The largest average mCG difference occurs in the CGI followed by the shores and then shelves (**Figure 3I**; Two-way ANOVA, main effect chromosome (XX v. XY)). While on average most CGIs are hypermethylated in XX (over XY) genotypes, there is a small subset of genes which show hypomethylation of CGIs in XX (vs. XY).

Similarly, gene bodies and the regions 4 kilobases upstream from the transcription start site (TSS) and 4 kb downstream of the transcription end site (TES) had higher mCG in XX than in XY genotypes (**Figure 3J**; Two-way ANOVA, main effect chromosome (XX v. XY)). The largest difference in mCG was in the regions 4 kilobases upstream from the transcription start site (TSS), inclusive of the gene promoter.

CCCTC-binding factor (*CTCF*) is a zinc-finger protein that mediates chromatin insulation and gene expression by binding 12- to 20-bp DNA motifs (CTCF binding sites) and altering the 3-dimensional chromatin structure. CTCF has high affinity for certain RNA transcripts, including *Xist* and anti-sense transcript *Tsix*,[67] which may help to differentially package the inactive and active X chromatin. In the FCG hippocampus, there is lower mCG in X Chromosome CTCF binding sites as compared to mCG on the whole X chromosome in all genotypes (XXF, XXM, XYF, XYM). There is higher mCG in XX hippocampi than XY, regardless of gonadal sex (**Figure 3K**). The magnitude of difference between XX and XY mCG in CTCF binding sites (~10%) is much greater than the average difference seen across the X chromosome (~3%).

Together, the methylation analysis of the X chromosome in FCG hippocampi suggests that X chromosome methylation is regulated by sex chromosome complement (XX v. XY) and likely not influenced by gonadal status.

X-chromosome differentially methylated regions (DMRs) by Whole Genome Oxidative Bisulfite Sequencing (WGoxBS) in FCG hippocampi.

After exploring the overall levels and patterning of DNA methylation on the X chromosome, mCG DMRs were called using 1 kb non-overlapping windows with minimum average difference of 10% between at least two groups (Chisq-test, sliding linear model (SLIM) $q<0.05$) and post-hoc Bonferroni corrected t-tests (XXF v. XYF, XXM v. XYM, XXF v. XXM, XYF v XYM) were used to assess pairwise differences. Using these criteria, we identified 1011 DMRs between XXF and XYF and 1367 DMRs between XXM and XYM, with 369 common DMRs (**Figure 4A**) on the X

chromosome. The 369 common DMRs appear to be evenly distributed across the X chromosome with some gaps containing no DMRs (**Figure 4B**). In agreement with the average difference in mCG (XX-XY) across the X chromosome, there are more hypermethylated DMRs in the XX genotypes as compared to the XY genotypes (**Figure 4C**). When the DMR methylation was higher in the XX genotypes, the XY genotypes had methylation values close to zero (**Figure 4D**). In cases where the XX genotypes had lower DMR methylation than the XY genotypes, the XY genotypes had methylation values close to 100% (**Figure 4D**). Sex-chromosomally driven DMRs were enriched in CGI, CGI shores, gene bodies, promoters, promoter flanking regions, CTCF binding sites, and simple repeats; DMRs were depleted in most repetitive elements (LINEs, SINES, LTRs) and open chromatin (**Figure 4E**).

Comparison of X chromosome gene expression and DNA methylation in FCG hippocampi.

DNA methylation regulates gene expression and genomic accessibility. The predominant theory in the field has been that methylation in gene promoters blocks the binding of transcription factors leading to repressed gene expression. In recent years, multiple additional theories of DNA modifications control of gene expression have been posited that include varied genomic regions (ie. distal regulatory elements, gene bodies) and cytosine context (mCG vs. mCH). Here we correlate DEG expression with gene body mCG and find significant negative associations with *Xist* (**Figure 4F**), *Flna* (**Figure 4G**), *Arhgap6* (**Figure 4H**), *Hccs* (**Figure 4I**).

Targeted bisulfite amplicon sequencing (BSAS) of X-chromosome gene promoters in FCG hippocampal DNA

Our WGoxBS data had 2-6X genome-wide coverage, which is sufficient to analyze methylation values in windows and collapse certain genomic regions. In order to assess base-specific methylation patterning, we performed targeted bisulfite amplicon sequencing (BSAS) within the promoter region of X-chromosome genes.

X-linked DEAD-box RNA helicase DDX3 (*Ddx3x*) plays an integral role in transcription and translation, as well as splicing and RNA transport. Mutations in *Ddx3x* have been associated with intellectual disability and developmental delays[46]. In our study, *Ddx3x* is more highly expressed in XX genotypes (XXF/XXM) as compared to XY genotypes (XYF/XYM). We amplified a region of the Ddx3x promoter, containing 4 CpG sites. The average mCG across that region was higher in XX genotypes as compared to XY genotypes, regardless of gonadal sex (**Figure 5A**). When examining the site-specific mCG across the amplified region of the *Ddx3x* promoter, all 4 mCG

sites have higher mCG in XX genotypes than XY genotypes (**Figure 5B**). The site-specific methylation appears to be strongly regulated by sex chromosome complement, as evidenced by the consistent topography of mCG.

Many of the consistently detected sexual dimorphisms on the X-chromosome are involved in maintenance of X-chromosome inactivation through cis-coating of the *Xist* transcript and the histone demethylase activities of *Kdm6a*, *Kdm5d*, and *Uty*. As such, both the X-chromosome gene expression and DNA methylation appear to be strongly regulated by sex chromosome complement. Although there were 2 genes (*Ace2*, *Aff1*) differentially expressed by sex, we did not find any examples of X-chromosome genomic features differentially methylated by gonadal sex (M v. F).

Following sex-chromosomally driven sex determination, development of the gonads and production of sex hormones further drives dichotomization of sexual phenotypes. In gonadal males, testes produce testosterone, an androgenic hormone[68]. Androgen receptor (*Ar*) is a hormone nuclear receptor and transcription factor that has many biological functions, including proper development of male reproductive organs and secondary sex characteristics[69]. Androgens have been found to effect hippocampal structure and function, as well as playing a role in hippocampal-dependent behavior, long-term potentiation, and dendritic arborization [70].

Ar is an X-chromosomally encoded gene and subject to X-chromosome inactivation. Although *Ar* was not differentially expressed by sex in outside studies (**Supplemental table 1 (Union)**) or in the present study (neither by sex (M v. F) or sex-chromosome complement (XX v. XY)), we wanted to determine if gonadal sex had any effect on *Ar* promoter methylation. BSAS analysis of 22 CpGs in the *Ar* promoter region, showed very low (~0%) mCG in XY genotypes with close to 40% average methylation in XX genotypes, regardless of gonadal sex (**Figure 5C**). Each CG-site within the amplified region of the *Ar* promoter has lower mCG (~0%) in XY genotypes compared to XX genotypes (~10-60%), regardless of gonadal sex. The patterning of *Ar* promoter mCG is well-conserved between XXF and XXM, suggesting tight regulation of *Ar* promoter methylation by sex chromosome complement, with no effect of gonadal sex (**Figure 5D**).

Toll-like receptor (*Tlr7*) is an X-encoded pattern recognition receptor (PRR), critical in innate immunity. Tlr7 recognizes single-stranded viral RNA (ssRNA)[71] and is primarily expressed on microglia in the brain[72]. In response to ssRNA, Tlr7 initiates a Type I interferon (IFN) response. Tlr7 was differentially expressed in outside studies (**Supplemental table 1 (Union)**) and by sex-chromosome complement in the present study (**Figure 2E**) with higher expression in XY (v. XX)

genotypes. The average mCG in an amplified region of the *Tlr7* promoter containing 4 CG sites is higher in XX genotypes over XY genotypes (**Figure 5E**). Three of the four CG sites within the amplified region were higher in XX genotypes as compared to the XY genotypes, with no differences by gonadal sex (**Figure 5F**).

Xist was one X-encoded gene that was differentially expressed by sex in all outside studies examined (**Supplemental table 1 (Intersect)**) and by sex chromosome complement in the present study (**Figure 1B,1E**). As a critical regulator of X-inactivation and X-chromosome dosage compensation, we analyzed mCG in an amplified region of the *Xist* promoter in FCG hippocampi. The average mCG within the amplified region of the *Xist* promoter was higher in XY genotypes than XX genotypes, regardless of their gonadal sex (**Figure 5G**). The base-specific topography of CG methylation is well conserved by sex chromosome complement (XX/XY), with no effect of gonadal sex (**Figure 5H**).

Angiotensin-converting enzyme 2 (Ace2) is surface receptor responsible for negative regulation of the renin-angiotensin system to modulate blood pressure and fluid/electrolyte balance. Ace2 recently gained attention as the entry receptor for the novel SARS-coronavirus 2 (SARS-CoV-2)[73]. Ace2 was differentially expressed by sex in the outside studies we examined (**Supplemental table 1 (Union)**) and by gonadal sex (M v. F) in the present study (**Figure 2G**). We assessed the mCG at a single CpG site within the Ace2 promoter and found higher mCG in XY genotypes as compared to XX genotypes, irrespective of their gonadal sex (**Figure 5I**).

In summary, targeted methylation analysis confirmed that X-chromosome methylation is tightly regulated, in a base-specific fashion, by sex chromosome complement, and not gonadal sex.

Transcriptomic analysis of autosomal differential expression from adult FCG hippocampi.

After establishing that the sex chromosome transcriptome and methylome of FCG hippocampi are primarily controlled by sex chromosome complement (XX v. XY), we examined autosomal regulation of sex differences. We first intersected the previous hippocampal transcriptomic studies to determine steady-state sex differences in the mouse hippocampus (**Figure 6A**). Although there were no sex differences in common between all studies (**Supplemental Table 2 (Intersection)**), there were 2896 sex differences identified in at least one study (**Supplemental Table 2 (Union)**). We next ran GO Biological Process Over-Representation Analysis (ORA) using WEB-based GEne SeT AnaLysis Toolkit (WebGestalt, www.webgestalt.org) on autosomal genes that were differentially expressed by sex in at least one outside study (**Supplemental Table 2 (Union)**). Enriched GO pathways were visualized on a reduced directed acyclic graph (DAG) (**Figure 6B**).

We identified 10 major GO terms, including cell-cell adhesion via plasma-membrane adhesion molecules, connective tissue development, epithelial cell proliferation, reproductive system development, urogenital system development, muscle system process, embryonic organ development, gliogenesis, multicellular organismal homeostasis, and pattern specification process (**Supplemental Table 3**).

We assessed autosomal sex differences in FCG hippocampus by sex chromosome complement (XX v. XY) and gonadal sex (M v. F) using directional RNA-Seq. After aligning, quantifying, and calling differentially expressed genes in StrandNGS software, 186 differentially expressed genes were identified: 62 genes differentially expressed by sex chromosome complement alone (XX v. XY), 123 genes differentially expressed by sex (M v. F), and 26 genes differentially expressed by both sex chromosome complement and gonadal sex (**Figure 6C**). Principal component analysis of differentially expressed autosomal genes shows separation by gonadal sex in component 1 and separation by sex chromosome complement in component 2 (**Figure 6D**). Hierarchical clustering of autosomal-encoded DEG shows proper clustering of samples by genotype (**Figure 6E**). ORA of the 37 chromosomally-driven (XX v. XY) sex differences in the FCG hippocampus revealed three pathways (synaptic vesicle cycle, nucleoside bisphosphate metabolic process, monoamine transport) enriched (FDR<0.05). Pathway analysis identified three pathways (response to protozoan, response to virus, antigen processing and presentation) differentially regulated by gonadal sex in the FCG hippocampus (FDR<0.05). Similar analysis of the 17 genes that were differentially expressed by sex chromosome complement and gonadal sex uncovered three pathways (response to protozoan, response to interferon beta, and response to virus) (**Figure 6F**).

Since we identified response to viruses and interferon-beta as pathways enriched in sex differences in the FCG hippocampus, we next further examined interferon-associated genes IRF-7 and IFIT-3. Interferon (IFN) is part of the innate immune system important in antiviral immunity. Upon viral recognition, production of IFN triggers the expression of IFN-stimulated genes (ISGs). IFN-beta is a type I IFN that is activated through PRRs[74], like Tlr7. In the brain, IFN-beta is primarily expressed by microglia[72]. In mouse models of AD, IFN was found to activate microglia leading to neuroinflammation and synaptic degradation. Blocking IFN signaling decreased microglia activation and concomitant synapse loss. Activation of IFN pathway was also observed in human AD[75].

Transcription factor IRF-7 is considered a “master regulator” in type-I IFN responses[76]. *Irf7* was differentially expressed by sex in one of the previously examined studies (**Supplemental Table**

2 (Union)). *Irf7* was also differentially expressed in our study by sex chromosome complement (XX v. XY) and gonadal sex (M v. F) in FCG hippocampus as evidenced by RNA-Seq (**Supplemental Table 3**) and RT-qPCR confirmation (**Figure 6G**). Interferon-induced protein with tetratricopeptide repeats 3 (IFIT3) is an antiviral RNA-binding protein which acts an intermediary in the activation of IRF-3 and upregulation of IFN-beta[77]. *Ifit3* was differentially expressed in one of the examined outside studies (**Supplemental Table 2 (Union)**). *Ifit3* was also differentially expressed by sex chromosome complement (XX v. XY) and gonadal sex (M v. F) in FCG hippocampus as evidenced by RNA-Seq (**Supplemental Table 3**) and RT-qPCR confirmation (**Figure 6H**).

Antigen processing and presentation was another pathway that was over-represented in our analysis of genes differentially expressed by gonadal sex in the FCG hippocampus. Microglia are the primary antigen presentation cells in the brain[78]. Class I major histocompatibility (MHC-I) complexes function in innate immune viral antigen presentation and detection. MHC-I components include B2m, H2-D1, and H2-K1. Previous studies from our lab identified sexually dimorphic induction of MHC-I with aging in the mouse and rat hippocampus[79,80]. Here we show differential expression of B2m by gonadal sex (**Figure 6J**) and H2-D1/H2-K1 by sex chromosome complement and gonadal sex (**Figure 6K-L**) in the FCG hippocampus (n=10-16/group, Two-Way ANOVA, main effect of sex chromosome complement (XX v. XY) or gonadal sex (M v. F)).

Autosomal chromosome levels of methylation in FCG hippocampus by WGoxBS

After analyzing autosomal sex differences in the FCG hippocampus, we assessed autosomal methylation in CG and CH context by WGoxBS. Overall, there were no differences in autosomal mCG (**Figure 7A**), with no difference in autosomal mCG in repetitive (**Figure 7B**) or non-repetitive (**Figure 7C**) elements. There also was no difference in average autosomal mCH (**Figure 7D**), with no difference in autosomal mCH in repetitive (**Figure 7E**) or non-repetitive (**Figure 7F**). There also were no apparent differences in autosomal mCG patterning across CGI, shores, and shelves (**Figure 7G**), gene bodies/flanking regions (**Figure 7H**), or CTCF-binding sites/flanking regions (**Figure 7I**).

Autosome differentially methylated regions (DMRs) by Whole Genome Oxidative Bisulfite Sequencing (WGoxBS) in FCG hippocampi.

After exploring the overall levels and patterning of DNA methylation on the autosomes, we called mCG DMRs using 1 kb non-overlapping windows with minimum average difference of 10% between at least two groups (Chisq-test, sliding linear model (SLIM) $q<0.05$) and post-hoc

Bonferroni corrected t-tests (XXF v. XYF, XXM v. XYM, XXF v. XXM, XYF v XYM, $p<\alpha=0.0125$) were used to assess pairwise differences. Using these criteria, we identified 2363 DMRs between XXF and XYF and 3031 DMRs between XXM and XYM, with 45 common sex chromosomally-regulated autosomal DMRs (**Figure 8A**). Hierarchical clustering of the DMRs showed three distinct clusters, with a set of 19 DMRs with higher mCG in XY genotypes (XY >XX), 25 DMRs with higher mCG in XX genotypes (XX>XY), and 1 discordant DMR (**Figure 8B**).

Sex-chromosomally driven autosomal DMRs were enriched in promoter flanking regions, enhancers, CTCF binding sites, and open chromatin; DMRs were depleted in CGIs, promoters, and repetitive elements (LINEs, LTRs) (**Figure 8C**). We identified 1055 DMRs between XXF and XXM and 1228 DMRs between XYF and XYM, with 17 common hormonally-regulated autosomal DMRs (**Figure 8D**). Hierarchical clustering of the hormonally-regulated DMRs showed three distinct clusters, with a set of 7 DMRs with higher mCG in females (F > M), 8 DMRs with higher mCG in XX (XX>XY), and 1 discordant DMR (**Figure 8E**). Similar to the chromosomally-regulated DMRs, hormonally-regulated DMRs are depleted in CGIs and repetitive elements (LINEs and LTRs) and enriched in promoter flanking regions (**Figure 8F**). GO Biological Process over-representation analysis of the autosomal DMRs differentially regulated by sex chromosome complement (XX v. XY) identified positive regulation of molecular function, trans-synaptic signaling, and cellular component pathways. Whereas, gonadal sex autosomal DMRs were overrepresented in lipid phosphorylation, regulation of neuron projection, and neurogenesis. DMRs differentially regulated by both sex chromosome and gonadal sex were over-represented in pathways involved in synaptic signaling, cell motility, and neurogenesis (**Figure 8G**). Thus, despite a strong immune-related transcriptomic signature, differential methylation appears to be mostly involved in neuron-related pathways. We believe that this is due to the relatively low percentage of microglia within the brain and warrants further cell-type specific studies focusing on microglia.

Discussion

The study of sex effects in brain health and disease have begun receiving the needed experimental attention in neuroscience studies. Not only do the sexual dimorphisms, differences, and divergences[81] need to be characterized but also the regulatory mechanisms giving rise to these sex effects. While hormonal mechanisms (both organizational and activational) have been the most studied, the potential regulation of sex effects by sex chromosomes, either independently, and in concert with hormones, has received relatively limited attention. Recent reports however, support the idea that sex chromosomal content is a central regulatory factor[82,83].

538 To begin characterizing the effects of sex chromosome content on epigenetic regulation of sex
539 chromosomes and autosomes, this study used the four core genotype (FCG) model[33] to examine
540 hippocampal DNA modifications and gene expression by gonadal sex (M vs F) and sex
541 chromosome content (XX vs XY) in roughly one-year old mice.

542 We first localized the translocation of *Sry* to an intergenic region of chromosome 3. This agrees
543 with prior imaging studies[41] and provides a precise location of the insertion. Importantly we also
544 found no evidence of other translocation sites in the genome. While there are ~13 copies of *Sry*
545 insertions of *Sry* they are not within an annotated gene. This could raise concerns about ectopic
546 Sry expression, but no evidence of Sry expression in the hippocampus was found, as would be
547 expected, providing evidence that normal tissue-specific regulation is occurring.

548 After performing paired transcriptomic and DNA methylation sequencing, a number of principle
549 findings were evident. For gene expression regulation, sex dimorphisms and differences in the
550 gene expression of X and Y encoded genes are principally driven by sex chromosome content
551 and not gonadal sex. Autosomally encoded gene expression differences are regulated by both
552 sex chromosomes and gonadal sex. While in a sense this may not be surprising, we are unaware
553 of prior data in the brain examining this point. The mechanism for this differential regulation may
554 lie, in part, in the X chromosome encoded histone demethylase Kdm6a and Y- encoded Uty and
555 Kdm5d as DEGs were enriched by H3-K27 and H3-K4 demethylation responsiveness. Future
556 work will need to manipulate individual X- and Y- encoded sexually dimorphic genes in the context
557 of the FCG model to determine the relative contributions of these to the autoregulation of the sex
558 chromosomes.

559 Analyses of hippocampal DNA methylation patterns across the XXF, XXM, XYM, and XYF
560 genome revealed a similar differential effect on autosomes and sex chromosomes. While whole
561 genome mCG levels did not vary by sex chromosome content or gonadal status, X chromosome
562 mCG in non-repetitive elements were lower in XYF and XYM compared to XX animals. This lower
563 level of mCG was also enriched in CpG Islands, promoter regions, and CTCF binding sites of the
564 X chromosome and likely reflects that XX mice have one inactive X (Xi). This interpretation is
565 bolstered by analysis of differentially methylated regions which are principally higher in XX vs XY
566 and correlate to mRNA expression of X encoded genes. Importantly this potential inactivation was
567 unaffected by gonadal status.

568 Conversely non-CpG methylation (mCH) was higher in XY versus XX mice irrespective of gonadal
569 status. Higher levels of X chromosome mCH have been reported in the liver[66] and have been

suggested to indicate Xi escape[84]. As these analyses were performed on tissue homogenates future studies will need to examine mCH in a cell type specific manner as mCH levels are much higher in neurons than other CNS cell types[84].

The patterns of autosomal DNA methylation by sex chromosome content and gonadal sex presented a very different profile. There were no overall differences in mCG or mCH levels. Rather differentially methylated regions were evident by both sex chromosome content and gonadal sex. Unlike the X chromosome, differences were not found in CGI regions but were most enriched in promoter flanking regions. Furthermore, differentially methylated regions were both higher and lower in comparisons by sex chromosome and gonadal sex unlike in the X chromosome which were almost uni-directional.

Taken together these findings are consistent with the hypothesis that the sex chromosomes have gonadal sex independent effects on the hippocampal epigenome and transcriptome. The use of the FCG mouse model allows for this demonstration for the first time in the brain. However, a number of questions remain to be answered in future studies. These principally consist of further controlling for gonadal hormone status but analyzing FCG mice that have be gonadectomized after development ~2-3 months of age. This will control for any activation hormonal differences between the genotypes. It is worth noting that these studies were conducted in adult mice ~12 months of age.

Most importantly for future studies, analysis of specific cell types is needed. The gene expression and epigenomic differences between neuronal, glial, and other cell types of the CNS is well described. Examining specific cell populations will increase the signal to noise from future molecular studies. Further investigation is highly warranted though given the significant effects of sex chromosome regulation of gene expression and DNA modification patterns in cis of the X chromosome and in trans of the autosomes.

Methods

Animals

All animal procedures were approved by the Institutional Animal Care and Use Committee at the University of Alabama at Birmingham (UAB) under protocol 21506. Four Core Genotypes mice on a C57Bl/6J background were obtained from the Jackson Laboratory where they were revitalized from frozen embryo stocks. Breeder pairs were set up with a XX female and a XY male, as described in the introduction. Pups were weaned into sex specific cages of 4-5 animals based on visual inspection of genitalia. Animals were maintained in an AAALAC approved UAB animal

facility at 21°C on a 12/12 light/dark cycle (lights on at 6:00am). Animals were provided ad libitum water and standard mouse chow (NIH31) until time of tissue collection, ~12 months of age for both males and females. Euthanasia prior to tissue harvesting was carried out by cervical dislocation followed by rapid decapitation. DNA was extracted from mouse hippocampus samples for genotyping using the primers: Sry (5′-AGC CCT ACA GCC ACA TGA TA-3′, 5′-GTC TTG CCT GTA TGT GAT GG-3′), Ymt (Y chromosome-specific sequence, 5′-CTG GAG CTC TAC AGT GAT GA-3′, 5′-CAG TTA CCA ATC AAC ACA TCA C-3′), and myogenin (5′-TTA CGT CCA TCG TGG ACA GCA T-3′, 5′-TGG GCT GGG TGT TAG TCT TAT-3′) [85].

High molecular weight (HWM) DNA isolation for pseudo long-read genomic sequencing

Hippocampi were dissected from XYF and XYM FCG mice (n=2/group), snap frozen in microfuge tubes with liquid nitrogen, and stored at -80ºC prior to DNA isolation. HMW DNA was extracted from fresh-frozen tissue according to 10X Genomics sample preparation protocol (https://support.10xgenomics.com/genome-exome/sample-prep/doc/demonstrated-protocol-hmw-dna-extraction-from-fresh-frozen-tissue). Frozen hippocampus from FCG mice was thawed on ice and minced with a razor blade. The tissue was gently dounce homogenized in 500 µL of Nuclei Isolation Buffer (Sigma Nuclei PURE Prep Kit: Lysis Buffer, 1 mM DTT, Sigma Nuclei PURE Prep Kit: 10% Triton X-100). After a brief centrifugation, the supernatant was transferred using a wide-bore pipette tip to a 2.0 mL round-bottom tube and centrifuged at 500 x g for 5 minutes. The supernatant was discarded, and pelleted nuclei were then resuspended in 70 µL of ice-cold PBS. To digest the nuclei, 10 µL of Proteinase K was added to the resuspended nuclei, followed by 70 µL ice-cold Digestion Buffer (20 mM EDTA, pH 11, 2mM Tris-HCl, pH 8.3,10 mM N-Laurylsarcosine sodium salt). Samples were rotated end-over-end for 2 hours at room temperature. To purify the DNA, Tween-20 was added to the sample to a final concentration of 0.1% and then 1X SPRISelect Reagent was added. The samples were rotated end-over end for 20 min. Tubes were placed in the DynaMag-2 magnetic rack to allow bead capture. After removing and discarding the supernatant, the beads were washed twice with 70% ethanol. The DNA was eluted from the beads with 50 µL Sample Elution Buffer (Qiagen AE Buffer, 0.1% Tween-20). Qubit dsDNA BR kit was used to quantify the DNA.

10X Linked-Read Library Preparation

Linked-read genomic libraries Chromium were constructed from 1 ng of HMW DNA from XYF and XYM (n=2/group) using Chromium Genome Library Prep Kit (#PN-120229, 10X Genomics, Pleasanton, CA), according to manufacturer's instructions. Briefly, following HMW gDNA

extraction 1 ng of HMW DNA was loaded onto a Chromium Genome Chip Kit (#PN-120216, 10X Genomics) for Gel Bead-in-Emulsions (GEM) generation and barcoding. After SPRISelect bead cleanup and library construction, libraries were normalized to 4 nM, pooled, and sequenced NextSeq500 (High PE150) in the OMRF Clinical Genomics Center (CGC).

Isolation of DNA/RNA from FCG hippocampi

Hippocampi were dissected from XXF, XXM, XYF, and XYM FCG mice (n=10-16/group), snap frozen in microfuge tubes with liquid nitrogen, and stored at -80ºC prior to DNA isolation. Nucleic acids (DNA/RNA) were isolated from flash-frozen tissues using the All Prep DNA/RNA Mini Kit (Qiagen, Germantown, MD) as previously described[86-88]. Briefly, 600 uL of Buffer RLT with beta-mercaptoethanol was added to the tube containing the frozen hippocampi. A steel bead was added to the tube and homogenized for 30 s at 30 Hz using a Tissue Lyser II (Qiagen). Homogenate was loaded onto a DNA spin column and the flow through supplemented with ethanol was loaded onto an RNA spin column. Columns were washed and nucleic acids eluted by centrifugation. Total DNA/RNA were quantified by Nanodrop (Thermofisher Scientific, Madison, USA). Quality of DNA and RNA were assessed by genomic and RNA screentapes, respectively, on a Tapestation 2200 (Agilent Technologies, Frankfurt, Germany). Only samples with RNA and DNA integrity numbers > 7 were used for subsequent experiments.

Digital PCR (dPCR) *Sry* copy number assay

Custom *Sry* fluorogenic copy number assays were designed and ordered from Integrated DNA Technologies (Coralville, IA) (Supplemental table 4). Mouse *Tert* fluorogenic copy number assay was used as a single copy gDNA control as reference (Life Technologies). DNA from FCG hippocampi (n=3/group) was used for dPCR, as previously[88], using the QuantStudio 3D Digital PCR kit (#A26361, ThermoFisher Scientific), according to manufacturer's instructions. After combining DNA with the Quantstudio 3D mastermix and *Sry* or *Tert* fluorogenic assay, reactions were loaded onto a Quantstudio 3D PCR chip with a Quantstudio 3D chip loader (#4482592, Thermofisher Scientific) and cycled on a GeneAmp PCR system 9700 with a flatblock attachment. Chips were read by the Quantstudio 3D chip reader (#4489084, Thermofisher Scientific) and analyzed using Quantstudio 3D AnalysisSuite cloud software V3.1.

Quantitative PCR (qPCR)

Confirmation of gene expression levels was performed with qPCR as previously described[43,89,90]. cDNA was synthesized with the ABI High-Capacity cDNA Reverse Transcription Kit (Applied

Biosystems Inc., Foster City, CA) from 25ng of purified RNA. qPCR was performed with gene-specific primer probe fluorogenic exonuclease assays (TaqMan, Life Technologies, Waltham, MA, **Supplemental table 4**) and the QuantStudio 12K Flex Real-Time PCR System (Applied Biosystems). Relative gene expression (RQ) was calculated with Expression Suite v 1.0.3 software using the $2^{-\Delta\Delta}$Ct analysis method with GAPDH as an endogenous control. Statistical analysis of the qPCR data was performed using GraphPad Prism 8 (San Diego, CA). Two-way ANOVA analyses were performed followed by the Tukey's multiple comparison test ($p<0.05$).

Library construction and RNA sequencing (RNA-seq)

Illumina's TruSeq Stranded mRNA Library Prep Kit (#20020594, Illumina) was used on 500 ng of total RNA for the preparation of strand-specific sequencing libraries according to manufacturer's guidelines. As previously described[44], rRNA depletion was performed prior to library construction.

RNA was isolated from fresh-frozen hippocampal tissue of 12 mo FCG mice (n=5-6/group), using Qiagen AllPrep DNA/RNA Mini Kit. After verifying RNA integrity numbers (RIN) with TapeStation (Agilent) and quantifying RNA with Qubit dsDNA Broad Range Assay kit (Invitrogen), 1 ug of RNA was used to construct RNA-Seq libraries using the Illumina TruSeq Stranded RNA Library Prep Kit, following the manufacturer's guidelines. cDNA libraries were sized by TapeStation (Agilent) and quantified by qPCR (KAPA Biosystems). Libraries were then normalized to 4 nM, pooled, denatured, and diluted for sequencing on Illumina Hiseq2500 in a 2x100 bp fashion.

RNA-Seq Data Analysis

Following sequencing, reads were trimmed, aligned, differential expression statistics and correlation analyses were performed in Strand NGS software package (Agilent), as previously described[43]. Reads were aligned against the Mm10 build of the mouse genome (2014.11.26). Alignment and filtering criteria included: adapter trimming, fixed 2bp trim from 5' and 6bp from 3' ends, a maximum number of one novel splice allowed per read, a minimum of 90% identity with the reference sequence, a maximum of 5% gap, trimming of 3' end with Q<30. Alignment was performed directionally with Read 1 aligned in reverse and Read 2 in forward orientation. Reads were filtered based on the mapping status and only those reads that aligned normally (in the appropriate direction) were retained. Normalization was performed with the DESeq algorithm[91]. Transcripts with an average read count value >20 in at least 100% of the samples in at least one group were considered expressed at a level sufficient for quantitation per tissue. Those transcripts below this level were considered not detected/not expressed and excluded, as these low levels of reads are close to background and are highly variable. A fold change >|1.25| cutoff was used

to eliminate those genes which were unlikely to be biologically significant and orthogonally confirmable due to their very small magnitude of change. For statistical analysis of differential expression, a two-way ANOVA with the factors of sex chromosome complement and gonadal sex and a Benjamini-Hochberg Multiple Testing Correction followed by Student-Newman Keuls post hoc test were used. Visualizations of hierarchical clustering and principal components analysis were performed in Strand Next Generation Analysis Software (NGS) (Version 3.1, Bangalore, India). The entirety of the sequencing data is available for download in FASTQ format from NCBI Sequence Read Archive (GEOXXXX).

Library construction and oxidative bisulfite sequencing (OxBS-seq)

DNA was isolated from fresh-frozen hippocampal tissue of 12 mo FCG mice (n=3/group), using Qiagen AllPrep DNA/RNA Mini Kit. Whole genome oxidative bisulfite sequencing libraries were prepared according to manufacturers guidelines (Ovation Ultralow Methyl-Seq Library System, Tecan Genomics, Inc., Redwood City, CA) as previously described[43,92]. Briefly, 1 µg of gDNA in 50 µl 1X low-EDTA TE buffer was sheared with a Covaris E220 sonicator (Covaris, Inc., Woburn, MA) to an average of 200 base pairs. Sheared products were sized by capillary electrophoresis (DNA HSD1000, Agilent) and cleaned using an Agencourt bead-based purification protocol. After quantifying (Qubit dsDNA, Thermofisher Scientific) the cleaned DNA, 200 ng gDNA fragments were prepared in a 12 µl volume to which 1µl of spike-in control DNA (0.08 ng/ul) with known levels of specific mC, hmC, and fC at individual sites was added. End repair, ligation of methylated adaptors (#L2V11DR-BC 1-96 adaptor plate, Tecan Genomics) and final repair were performed according to manufacturer's instructions. Normalized DNA was oxidized and then bisulfite- converted with the True Methyl oxBS module (NuGEN) with desulfonation and purification. 22 µl of libraries were eluted from the magnetic beads. qPCR was used to determine the number (N) of PCR cycles required for library amplification. Oxidative bisulfite-converted samples were amplified for 13 cycles [95° C- 2 min, N (95°C-15 s, 60°C-1 min, 72° C-30s)]. Amplified libraries were purified with Agencourt beads and eluted in low-EDTA TE buffer. Capillary electrophoresis (TapeStation HSD1000, Agilent) was used to validate and quantify libraries. Amplified libraries were normalized to a concentration of 4 nM and pooled, denatured, and diluted to 12 pM for sequencing on NovaSeq 6000 (Illumina) according to manufacturer's guidelines with the exception of a custom sequencing primer (MetSeq Primer) that was spiked in with the Illumina Read 1 primer to a final concentration of 0.5 µM.

OxBS-seq data analysis

Global levels of mCG, hmCG, and mCH were analyzed as previously described[43,92] Before aligning, paired-end reads were adaptor-trimmed and filtered using Trimmomatic[93] 0.35. End-trimming removed leading and trailing bases with Q-score<25, cropped 4 bases from the start of the read, dropped reads less than 25 bases long, and dropped reads with average Q-score<25. Unpaired reads after trimming were not considered for alignment. Alignment of trimmed OxBS-converted sequences was carried out using Bismark[94] 0.16.3 with Bowtie 2[95] against the mouse reference genome (GRCm38/mm10). Bams were de-duplicated using Bismark. Methylation call percentages for each CpG and non-CpG (CH) site within the genome were calculated by dividing the methylated counts over the total counts for that site in the oxidative bisulfite - converted libraries (OXBS). Genome-wide CpG and CH methylation levels were calculated separately. BAM files generated during alignment were run through MethylKit in R[96] to generate context-specific (CpG/CH) coverage text files. Bisulfite conversion efficiency for C, mC, and hmC was estimated using CEGX spike-in control sequences. Untrimmed fastq files were run through CEGX QC v0.2, which output a fastqc_data.txt file containing the conversion mean for C, mC, and hmC.

DMR Analysis

CpG text files were read into methylKit v XXXX and converted to an object. The mouse genome was tiled in 200 nt non-overlapping windows. Each window was filtered for a minimum count of 10. Samples were then united and compared for windows covered in all samples. Differentially methylated regions (DMRs) were called using default parameters. DMRs were filtered to differences that were >5% different between at least two groups and had a SLIM-generated q-value less than 0.05. There were 13010 windows that met these criteria. The methylDiff object was intersected with the methylBase object to calculate the % methylation for each window that passed the described filtering. Next, 4 pairwise t-tests (XXF v XYF, XXM v XYM, XXF v XXM, XYF v. XYM) were conducted and corrected for the four comparisons using BHMTC and an alpha<0.05.

References

1. Yagi, S. & Galea, L.A.M. Sex differences in hippocampal cognition and neurogenesis. *Neuropsychopharmacology* **44**, 200-213 (2019).
2. Eggers, S. & Sinclair, A. Mammalian sex determination-insights from humans and mice. *Chromosome Res* **20**, 215-238 (2012).
3. Phoenix, C.H., Goy, R.W., Gerall, A.A. & Young, W.C. Organizing action of prenatally administered testosterone propionate on the tissues mediating mating behavior in the female guinea pig. *Endocrinology* **65**, 369-382 (1959).
4. Moghadami, S., Jahanshahi, M., Sepehri, H. & Amini, H. Gonadectomy reduces the density of androgen receptor-immunoreactive neurons in male rat's hippocampus: testosterone replacement compensates it. *Behavioral and Brain Functions* **12**, 5 (2016).
5. Kokras, N.*, et al.* Sex differences in behavioral and neurochemical effects of gonadectomy and aromatase inhibition in rats. *Psychoneuroendocrinology* **87**, 93-107 (2018).
6. Farquhar, C.E.*, et al.* Sex, THC, and hormones: Effects on density and sensitivity of CB(1) cannabinoid receptors in rats. *Drug Alcohol Depend* **194**, 20-27 (2019).
7. Mitsushima, D., Takase, K., Takahashi, T. & Kimura, F. Activational and organisational effects of gonadal steroids on sex-specific acetylcholine release in the dorsal hippocampus. *J Neuroendocrinol* **21**, 400-405 (2009).
8. Wu, Y.C., Du, X., van den Buuse, M. & Hill, R.A. Sex differences in the adolescent developmental trajectory of parvalbumin interneurons in the hippocampus: a role for estradiol. *Psychoneuroendocrinology* **45**, 167-178 (2014).
9. Ramzan, F., Azam, A.B., Monks, D.A. & Zovkic, I.B. Androgen receptor is a negative regulator of contextual fear memory in male mice. *Horm Behav* **106**, 10-18 (2018).
10. McQueen, J.K., Dow, R.C. & Fink, G. Gonadal steroids regulate number of astrocytes immunostained for glial fibrillary acidic protein in mouse hippocampus. *Mol Cell Neurosci* **3**, 482-486 (1992).
11. Arnold, A.P. Conceptual frameworks and mouse models for studying sex differences in physiology and disease: why compensation changes the game. *Exp Neurol* **259**, 2-9 (2014).
12. Mulnard, R.A.*, et al.* Estrogen Replacement Therapy for Treatment of Mild to Moderate Alzheimer DiseaseA Randomized Controlled Trial. *JAMA* **283**, 1007-1015 (2000).
13. Fang, H., Disteche, C.M. & Berletch, J.B. X Inactivation and Escape: Epigenetic and Structural Features. *Front Cell Dev Biol* **7**, 219 (2019).
14. Knickmeyer, R.C. & Davenport, M. Turner syndrome and sexual differentiation of the brain: implications for understanding male-biased neurodevelopmental disorders. *J Neurodev Disord* **3**, 293-306 (2011).
15. Harris, V.M.*, et al.* Klinefelter's syndrome (47,XXY) is in excess among men with Sjogren's syndrome. *Clin Immunol* **168**, 25-29 (2016).
16. Arnold, A.P. A general theory of sexual differentiation. *Journal of Neuroscience Research* **95**, 291-300 (2017).
17. Panning, B. X-chromosome inactivation: the molecular basis of silencing. *Journal of Biology* **7**, 30 (2008).
18. Fang, H., Disteche, C.M. & Berletch, J.B. X Inactivation and Escape: Epigenetic and Structural Features. *Front Cell Dev Biol* **7**, 219-219 (2019).
19. Carrel, L. & Willard, H.F. X-inactivation profile reveals extensive variability in X-linked gene expression in females. *Nature* **434**, 400-404 (2005).
20. Berletch, J.B., Yang, F., Xu, J., Carrel, L. & Disteche, C.M. Genes that escape from X inactivation. *Human Genetics* **130**, 237-245 (2011).

21. Mousavi, M.J., Mahmoudi, M. & Ghotloo, S. Escape from X chromosome inactivation and female bias of autoimmune diseases. *Molecular Medicine* **26**, 127 (2020).
22. Youness, A., Miquel, C.-H. & Guéry, J.-C. Escape from X Chromosome Inactivation and the Female Predominance in Autoimmune Diseases. *Int J Mol Sci* **22**, 1114 (2021).
23. Bajic, V.P.*, et al.* The X Files: "The Mystery of X Chromosome Instability in Alzheimer's Disease". *Front Genet* **10**, 1368-1368 (2020).
24. Mangold, C.A.*, et al.* CNS-wide Sexually Dimorphic Induction of the Major Histocompatibility Complex 1 Pathway With Aging. *The Journals of Gerontology: Series A* **72**, 16-29 (2017).
25. Masser, D.R.*, et al.* Sexually divergent DNA methylation patterns with hippocampal aging. *Aging Cell* **16**, 1342-1352 (2017).
26. Vied, C.*, et al.* Transcriptomic analysis of the hippocampus from six inbred strains of mice suggests a basis for sex-specific susceptibility and severity of neurological disorders. *J Comp Neurol* **524**, 2696-2710 (2016).
27. Bundy, J.L., Vied, C. & Nowakowski, R.S. Sex differences in the molecular signature of the developing mouse hippocampus. *BMC Genomics* **18**, 237-237 (2017).
28. Xia, Y.*, et al.* Sex-differential DNA methylation and associated regulation networks in human brain implicated in the sex-biased risks of psychiatric disorders. *Mol Psychiatry* **26**, 835-848 (2021).
29. Arnold, A.P. Mouse models for evaluating sex chromosome effects that cause sex differences in non-gonadal tissues. *J Neuroendocrinol* **21**, 377-386 (2009).
30. De Vries, G.J.*, et al.* A model system for study of sex chromosome effects on sexually dimorphic neural and behavioral traits. *J Neurosci* **22**, 9005-9014 (2002).
31. Markham, J.A.*, et al.* Sex differences in mouse cortical thickness are independent of the complement of sex chromosomes. *Neuroscience* **116**, 71-75 (2003).
32. Wagner, C.K.*, et al.* Neonatal mice possessing an Sry transgene show a masculinized pattern of progesterone receptor expression in the brain independent of sex chromosome status. *Endocrinology* **145**, 1046-1049 (2004).
33. Arnold, A.P. & Chen, X. What does the "four core genotypes" mouse model tell us about sex differences in the brain and other tissues? *Front Neuroendocrinol* **30**, 1-9 (2009).
34. Carruth, L.L., Reisert, I. & Arnold, A.P. Sex chromosome genes directly affect brain sexual differentiation. *Nat Neurosci* **5**, 933-934 (2002).
35. Gioiosa, L.*, et al.* Sex chromosome complement affects nociception in tests of acute and chronic exposure to morphine in mice. *Horm Behav* **53**, 124-130 (2008).
36. Chen, X.*, et al.* Sex difference in neural tube defects in p53-null mice is caused by differences in the complement of X not Y genes. *Dev Neurobiol* **68**, 265-273 (2008).
37. Smith-Bouvier, D.L.*, et al.* A role for sex chromosome complement in the female bias in autoimmune disease. *J Exp Med* **205**, 1099-1108 (2008).
38. Davis, E.J., Lobach, I. & Dubal, D.B. Female XX sex chromosomes increase survival and extend lifespan in aging mice. *Aging Cell* **18**, e12871-e12871 (2019).
39. Davis, E.J.*, et al.* A second X chromosome contributes to resilience in a mouse model of Alzheimer's disease. *Science Translational Medicine* **12**, eaaz5677 (2020).
40. Kashimada, K. & Koopman, P. Sry: the master switch in mammalian sex determination. *Development* **137**, 3921-3930 (2010).
41. Itoh, Y.*, et al.* Four core genotypes mouse model: localization of the Sry transgene and bioassay for testicular hormone levels. *BMC Res Notes* **8**, 69 (2015).
42. Bundy, J.L., Vied, C. & Nowakowski, R.S. Sex differences in the molecular signature of the developing mouse hippocampus. *BMC Genomics* **18**, 237 (2017).

43. Chucair-Elliott, A.J., *et al.* Tamoxifen induction of Cre recombinase does not cause long-lasting or sexually divergent responses in the CNS epigenome or transcriptome: implications for the design of aging studies. *GeroScience* (2019).
44. Hadad, N., Masser, D.R., Blanco-Berdugo, L., Stanford, D.R. & Freeman, W.M. Early-life DNA methylation profiles are indicative of age-related transcriptome changes. *Epigenetics Chromatin* **12**, 58 (2019).
45. Berletch, J.B., *et al.* Escape from X Inactivation Varies in Mouse Tissues. *PLOS Genetics* **11**, e1005079 (2015).
46. Snijders Blok, L., *et al.* Mutations in DDX3X Are a Common Cause of Unexplained Intellectual Disability with Gender-Specific Effects on Wnt Signaling. *Am J Hum Genet* **97**, 343-352 (2015).
47. Hu, H., *et al.* X-exome sequencing of 405 unresolved families identifies seven novel intellectual disability genes. *Mol Psychiatry* **21**, 133-148 (2016).
48. Shpargel, K.B., Sengoku, T., Yokoyama, S. & Magnuson, T. UTX and UTY Demonstrate Histone Demethylase-Independent Function in Mouse Embryonic Development. *PLOS Genetics* **8**, e1002964 (2012).
49. Cerase, A., Pintacuda, G., Tattermusch, A. & Avner, P. Xist localization and function: new insights from multiple levels. *Genome Biology* **16**, 166 (2015).
50. Mizukami, H., *et al.* KDM5D-mediated H3K4 demethylation is required for sexually dimorphic gene expression in mouse embryonic fibroblasts. *J Biochem* **165**, 335-342 (2019).
51. Ramathal, C., *et al.* DDX3Y gene rescue of a Y chromosome AZFa deletion restores germ cell formation and transcriptional programs. *Scientific Reports* **5**, 15041 (2015).
52. Marks, H., *et al.* High-resolution analysis of epigenetic changes associated with X inactivation. *Genome Res* **19**, 1361-1373 (2009).
53. Tate, P.H. & Bird, A.P. Effects of DNA methylation on DNA-binding proteins and gene expression. *Curr Opin Genet Dev* **3**, 226-231 (1993).
54. Jones, P.L., *et al.* Methylated DNA and MeCP2 recruit histone deacetylase to repress transcription. *Nat Genet* **19**, 187-191 (1998).
55. Watanabe, S., *et al.* Methylated DNA-binding domain 1 and methylpurine-DNA glycosylase link transcriptional repression and DNA repair in chromatin. *Proc Natl Acad Sci U S A* **100**, 12859-12864 (2003).
56. Fujita, N., *et al.* Methyl-CpG binding domain 1 (MBD1) interacts with the Suv39h1-HP1 heterochromatic complex for DNA methylation-based transcriptional repression. *J Biol Chem* **278**, 24132-24138 (2003).
57. Brackertz, M., Boeke, J., Zhang, R. & Renkawitz, R. Two highly related p66 proteins comprise a new family of potent transcriptional repressors interacting with MBD2 and MBD3. *J Biol Chem* **277**, 40958-40966 (2002).
58. Razin, A. & Cedar, H. DNA methylation and genomic imprinting. *Cell* **77**, 473-476 (1994).
59. Wolf, S.F., Jolly, D.J., Lunnen, K.D., Friedmann, T. & Migeon, B.R. Methylation of the hypoxanthine phosphoribosyltransferase locus on the human X chromosome: implications for X-chromosome inactivation. *Proceedings of the National Academy of Sciences* **81**, 2806-2810 (1984).
60. Pfeifer, G.P., Steigerwald, S.D., Hansen, R.S., Gartler, S.M. & Riggs, A.D. Polymerase Chain Reaction-Aided Genomic Sequencing of an X Chromosome- Linked CpG Island: Methylation Patterns Suggest Clonal Inheritance, CpG Site Autonomy, and an Explanation of Activity State Stability. *Proc Natl Acad Sci U S A* **87**, 8252-8256 (1990).
61. Bartlett, M.H., Adra, C.N., Park, J., Chapman, V.M. & McBurney, M.W. DNA methylation of two X chromosome genes in female somatic and embryonal carcinoma cells. *Somatic Cell and Molecular Genetics* **17**, 35-47 (1991).

62. Angrisano, T., *et al.* TACC3 mediates the association of MBD2 with histone acetyltransferases and relieves transcriptional repression of methylated promoters. *Nucleic Acids Res* **34**, 364-372 (2006).
63. Sharp, A.J., *et al.* DNA methylation profiles of human active and inactive X chromosomes. *Genome Res* **21**, 1592-1600 (2011).
64. Chucair-Elliott, A.J., *et al.* Tamoxifen induction of Cre recombinase does not cause long-lasting or sexually divergent responses in the CNS epigenome or transcriptome: implications for the design of aging studies. *Geroscience* **41**, 691-708 (2019).
65. Jeziorska, D.M., *et al.* DNA methylation of intragenic CpG islands depends on their transcriptional activity during differentiation and disease. *Proceedings of the National Academy of Sciences* **114**, E7526-E7535 (2017).
66. Duncan, C.G., *et al.* Dosage compensation and DNA methylation landscape of the X chromosome in mouse liver. *Scientific Reports* **8**, 10138 (2018).
67. Kung, J.T., *et al.* Locus-specific targeting to the X chromosome revealed by the RNA interactome of CTCF. *Mol Cell* **57**, 361-375 (2015).
68. Cortes, L.R., Cisternas, C.D. & Forger, N.G. Does Gender Leave an Epigenetic Imprint on the Brain? *Frontiers in Neuroscience* **13**(2019).
69. Davey, R.A. & Grossmann, M. Androgen Receptor Structure, Function and Biology: From Bench to Bedside. *Clin Biochem Rev* **37**, 3-15 (2016).
70. Atwi, S., McMahon, D., Scharfman, H. & MacLusky, N.J. Androgen Modulation of Hippocampal Structure and Function. *Neuroscientist* **22**, 46-60 (2016).
71. Kawasaki, T. & Kawai, T. Toll-like receptor signaling pathways. *Front Immunol* **5**, 461 (2014).
72. Zhang, Y., *et al.* An RNA-Sequencing Transcriptome and Splicing Database of Glia, Neurons, and Vascular Cells of the Cerebral Cortex. *The Journal of Neuroscience* **34**, 11929 (2014).
73. Hikmet, F., *et al.* The protein expression profile of ACE2 in human tissues. *Molecular Systems Biology* **16**, e9610 (2020).
74. Blank, T. & Prinz, M. Type I interferon pathway in CNS homeostasis and neurological disorders. *Glia* **65**, 1397-1406 (2017).
75. Roy, E.R., *et al.* Type I interferon response drives neuroinflammation and synapse loss in Alzheimer disease. *The Journal of Clinical Investigation* **130**, 1912-1930 (2020).
76. Honda, K., *et al.* IRF-7 is the master regulator of type-I interferon-dependent immune responses. *Nature* **434**, 772-777 (2005).
77. Liu, X.-Y., Chen, W., Wei, B., Shan, Y.-F. & Wang, C. IFN-Induced TPR Protein IFIT3 Potentiates Antiviral Signaling by Bridging MAVS and TBK1. *The Journal of Immunology* **187**, 2559 (2011).
78. Schetters, S.T.T., Gomez-Nicola, D., Garcia-Vallejo, J.J. & Van Kooyk, Y. Neuroinflammation: Microglia and T Cells Get Ready to Tango. *Front Immunol* **8**, 1905 (2017).
79. VanGuilder Starkey, H.D., *et al.* Neuroglial expression of the MHCI pathway and PirB receptor is upregulated in the hippocampus with advanced aging. *J Mol Neurosci* **48**, 111-126 (2012).
80. Mangold, C.A., *et al.* CNS-wide Sexually Dimorphic Induction of the Major Histocompatibility Complex 1 Pathway With Aging. *J Gerontol A Biol Sci Med Sci* **72**, 16-29 (2017).
81. McCarthy, M.M., Arnold, A.P., Ball, G.F., Blaustein, J.D. & De Vries, G.J. Sex differences in the brain: the not so inconvenient truth. *J Neurosci* **32**, 2241-2247 (2012).
82. Davis, E.J., *et al.* A second X chromosome contributes to resilience in a mouse model of Alzheimer's disease. *Sci Transl Med* **12**(2020).
83. Qi, S., *et al.* X chromosome escapee genes are involved in ischemic sexual dimorphism through epigenetic modification of inflammatory signals. *J Neuroinflammation* **18**, 70 (2021).
84. Lister, R., *et al.* Global epigenomic reconfiguration during mammalian brain development. *Science* **341**, 1237905 (2013).

85. Coppe, J.P., Desprez, P.Y., Krtolica, A. & Campisi, J. The senescence-associated secretory phenotype: the dark side of tumor suppression. *Annu Rev Pathol* **5**, 99-118 (2010).
86. Ansere, V.A.*, et al.* Cellular hallmarks of aging emerge in the ovary prior to primordial follicle depletion. *Mech Ageing Dev* **194**, 111425 (2021).
87. Masser, D.R., Berg, A.S. & Freeman, W.M. Focused, high accuracy 5-methylcytosine quantitation with base resolution by benchtop next-generation sequencing. *Epigenetics & chromatin* **6**, 33-33 (2013).
88. Masser, D.R., Clark, N.W., Van Remmen, H. & Freeman, W.M. Loss of the antioxidant enzyme CuZnSOD (Sod1) mimics an age-related increase in absolute mitochondrial DNA copy number in the skeletal muscle. *Age (Dordr)* **38**, 323-333 (2016).
89. Simpson, J.T.*, et al.* Detecting DNA cytosine methylation using nanopore sequencing. *Nature Methods* **14**, 407 (2017).
90. Masser, D.R.*, et al.* Hippocampal subregions exhibit both distinct and shared transcriptomic responses to aging and nonneurodegenerative cognitive decline. *J Gerontol A Biol Sci Med Sci* **69**, 1311-1324 (2014).
91. Anders, S. & Huber, W. Differential expression analysis for sequence count data. *Genome Biol* **11**, R106 (2010).
92. Chucair-Elliott, A.J.*, et al.* Inducible cell-specific mouse models for paired epigenetic and transcriptomic studies of microglia and astroglia. *Communications Biology* **3**, 693 (2020).
93. Bolger, A.M., Lohse, M. & Usadel, B. Trimmomatic: a flexible trimmer for Illumina sequence data. *Bioinformatics* **30**, 2114-2120 (2014).
94. Krueger, F. & Andrews, S.R. Bismark: a flexible aligner and methylation caller for Bisulfite-Seq applications. *Bioinformatics* **27**, 1571-1572 (2011).
95. Langmead, B. & Salzberg, S.L. Fast gapped-read alignment with Bowtie 2. *Nat Methods* **9**, 357-359 (2012).
96. Akalin, A.*, et al.* methylKit: a comprehensive R package for the analysis of genome-wide DNA methylation profiles. *Genome Biol* **13**, R87 (2012).

Author contributions

Sarah R. Ocañas: first author, design of the study, execution of experiments, data acquisition, analysis, and interpretation, figure generation, manuscript writing and preparation

Victor A. Ansere: execution of experiments, data acquisition, analysis, and interpretation, figure generation, manuscript preparation

Kyla B. Tooley: execution of experiments, data acquisition, analysis, and interpretation, figure generation, manuscript preparation

Niran Hadad: data analysis and interpretation, figure generation

Ana J. Chucair-Elliott: design of the study, data interpretation, manuscript preparation

David R. Stanford: design of the study, data analysis and interpretation

Shannon Rice: execution of experiments, data acquisition, analysis, and interpretation

Benjamin Wronowski: execution of experiments, data acquisition, analysis, and interpretation, figure generation

Jessica M. Hoffman: design of the study, execution of experiments, data analysis and interpretation, manuscript writing and preparation

Steven N. Austad: design of the study, data analysis and interpretation, manuscript writing and preparation

Michael B. Stout: design of the study, execution of experiments, data acquisition, analysis, and interpretation, manuscript writing and preparation

Willard M. Freeman: Corresponding author, design of the study, data analysis and interpretation, figure generation, manuscript writing, preparation, and submission.

Competing Interest statements

Sarah R. Ocañas: None

Victor A. Ansere: None

Kyla B. Tooley: None

Niran Hadad: None

Ana J. Chucair-Elliott: None

David R. Stanford: None

Shannon Rice: None

Benjamin Wronowski: None

Jessica M. Hoffman: None

Steven N. Austad: None

Michael B. Stout: None

Willard M. Freeman: None

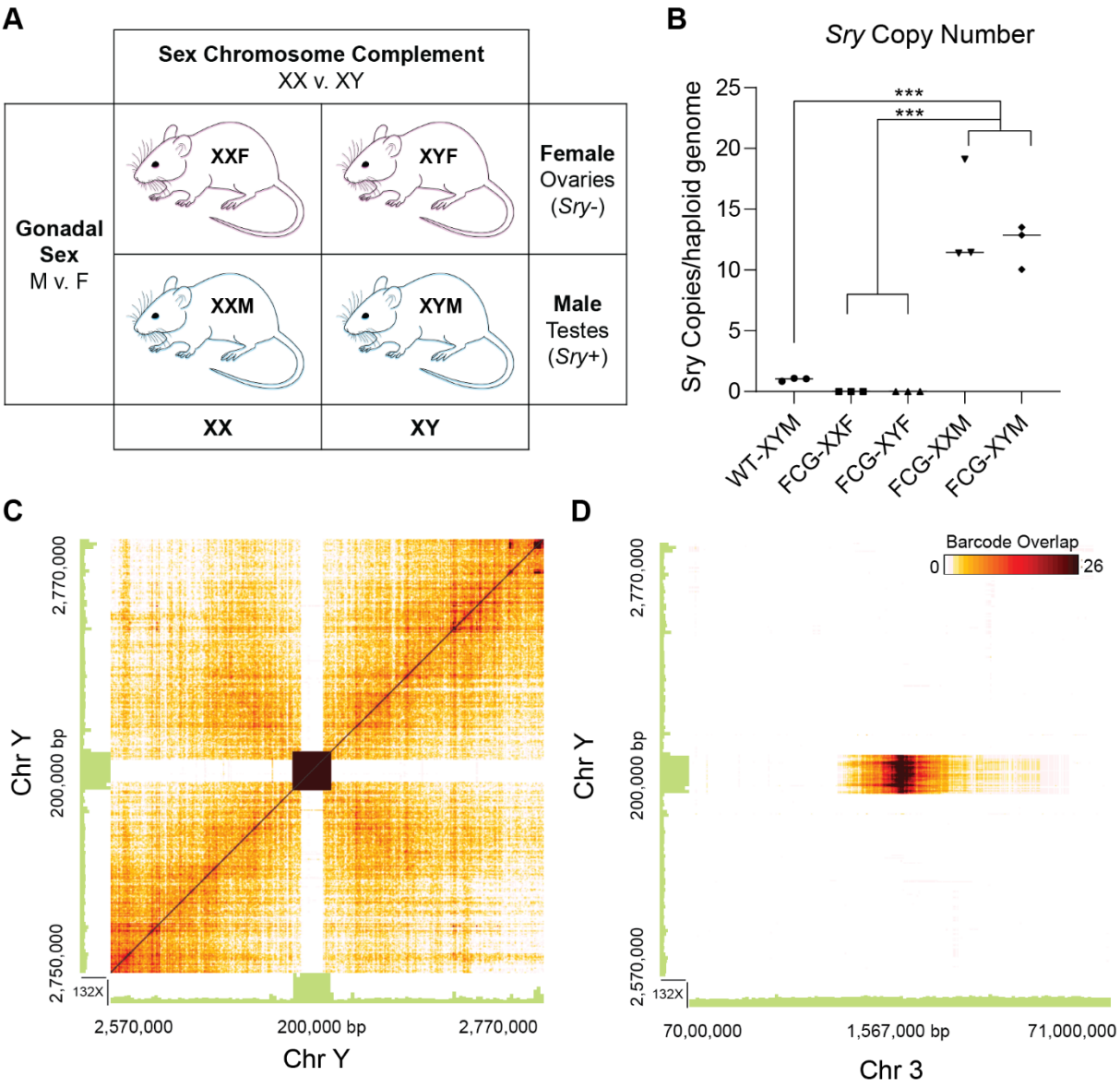

Figure 1. *Sry* copy number and localization in FCG hippocampi. DNA isolated from FCG and wild type hippocampi (n=3/group) was used for digital PCR *Sry* copy number and 10X genomics linked read sequencing. A) FCG "sex-reversal" mouse model two-way design to study hormonal and chromosomal contributions to sex effects. B) Wildtype (WT) C57BL/6 mice have one copy of the testis-determining *Sry* gene, while FCG males (both XX and XY) have 12-14 copies of *Sry*. *Sry* was not detected in the FCG females. C) Linked read sequencing of FCG XYM, shows strong linkage of the *Sry* gene to itself, but not to adjacent regions of the Y chromosome (Chr Y). D) *Sry* gene shows strong linkage to a region on Chromosome 3 (Chr 3).

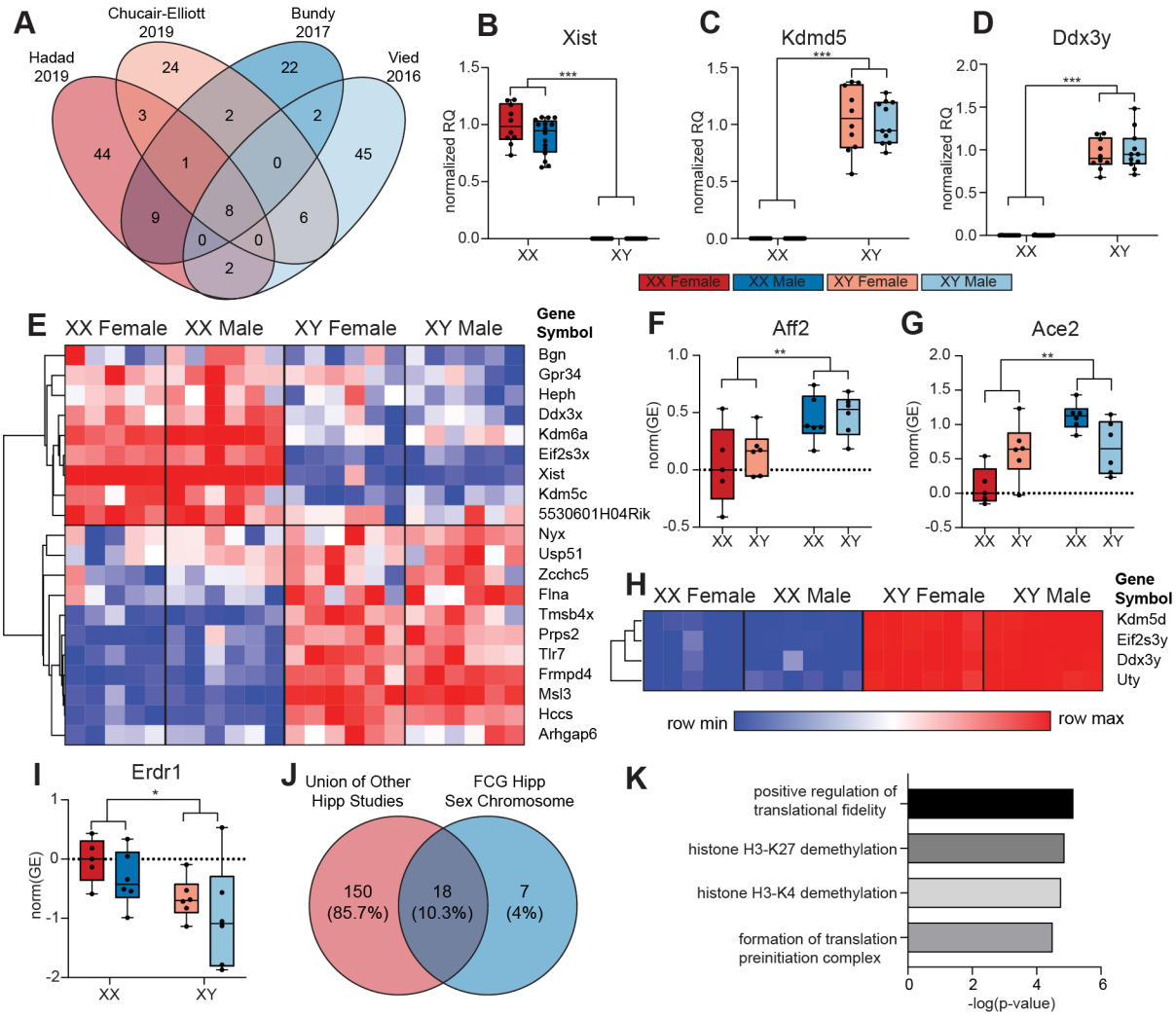

Figure 2. Transcriptomic analysis of sex chromosomal driven differential expression of sex chromosome encoded genes in adult FCG hippocampi. DNA and RNA were isolated from FCG hippocampi (n=10-16/group). mRNA expression was assessed by RT-qPCR (n=10-16/group) and stranded RNA-Seq (n=6/group). Results were compared to previously published hippocampal transcriptomic sex differences. **Boxplots** represent median, interquartile range, and minimum/maximum normalized gene expression. A) Comparison of four previous hippocampal transcriptomic studies, shows 168 sex chromosome-encoded sex differences in wild-type mice across studies with eight genes common between all studies (*Xist Ddx3x, Kdm6a, Eif2s3x, Kdm5d, Eif2s3y, Uty, Ddx3y)* B) In the FCG hippocampus, RT-qPCR of X-chromosome encoded gene *Xist* confirms differential expression by sex chromosome (XX vs. XY) but not sex (M v. F) (Two-way ANOVA, main effect of sex-chromosome complement (XX v. XY), ***p<0.001) . C-D) RT-qPCR of Y-chromosome encoded genes shows similar levels of expression of (C) *Kdm5d* and (D) *Ddx3y* in XYM and XYF, and no detectable expression in XXM or XXF (Two-way ANOVA, main effect of sex-chromosome complement (XX v. XY), ***p<0.001). E) RNA-Seq analysis of X-chromosome encoded genes showed 20 genes that are differentially expressed by sex chromosome (XX vs. XY) but not by sex (M v. F). F-G) RNA-seq analysis of X chromosome genes revealed only two genes (*Aff2, Ace2*) differentially expressed by sex (M v. F) and not by sex chromosome complement. Both (F) *Aff2* and (G) *Ace2* had higher expression in males than females regardless of their sex chromosome (Two-way ANOVA, main effect of gonadal sex (M v. F), **p<0.01). H-I) RNA-Seq analysis of Y chromosome encoded genes identified 5 differentially expressed genes by sex chromosome (XX vs. XY) but not by sex (M v. F).

There were no Y chromosome genes that were differentially expressed by sex (M v. F). H) Four of the genes (*Kdm5d, Eif2s3y, Ddx3y, Uty*) show no expression in XX genotypes. I) Located in the pseudo autosomal region (PAR) of the X/Y-chromsomes, *Erdr1* shows higher expression in XX genotype. J) Comparing the union of previous hippocampal studies described in (A) to the FCG sex chromosome genes differentially expressed between XX and XY genotypes, yields 18 common genes. K) GO Ontology analysis of the 18 genes from (J), identified four significantly enriched biological pathways

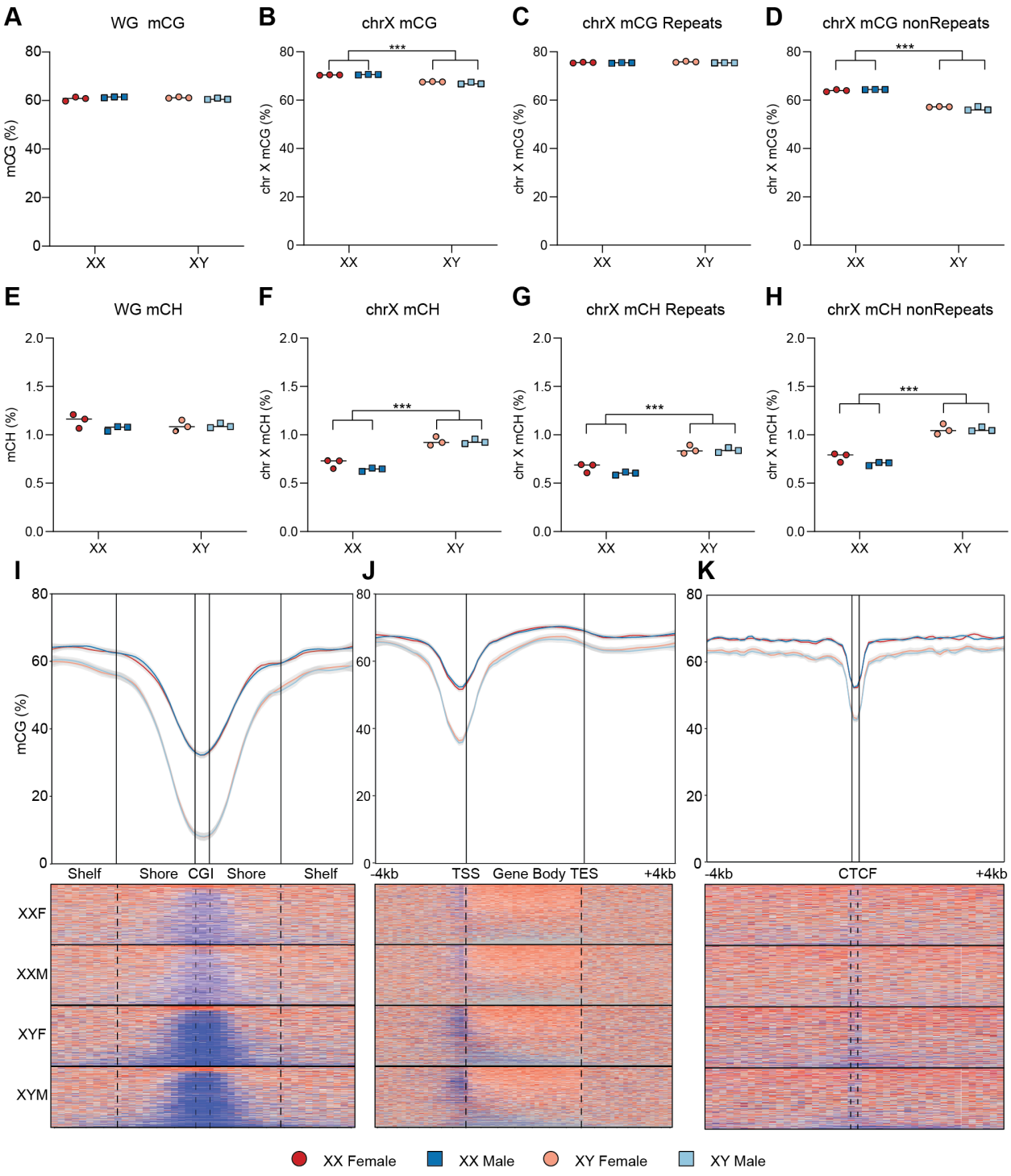

Figure 3. X chromosome levels of methylation in FCG hippocampus by WGoxBS. DNA was isolated from FCG hippocampi (n=3/group). Methylation in CpG (CG) and non-CpG (CH) contexts was assessed by WGoxBS (n=3/group). A) There is no main effect difference in overall whole genome (WG) levels of methylation in CG context (mCG) (Two-way ANOVA). B) XX mice have higher levels of X chromosome mCG than XY mice regardless of gonadal sex (M v. F). The differences in X-chromosome mCG are concentrated in non-repetitive elements, as there is: (C) no difference in mCG in repetitive elements and (D) higher

levels of mCG in XX mice as compared to XY mice regardless of their gonadal sex (M v. F). E) There is no main effect difference in overall levels of methylation in non-CpG context (mCH) (Two-way ANOVA). F) XX mice have lower mCH than XY mice specifically on the X chromosome, regardless of their gonadal sex (M v. F). The differences in X-chromosome mCH are seen in both (E) repetitive and (F) non-repetitive elements of the genome. mCG levels were calculated with respect to genic regions by binning 200 nucleotides in flanking regions and region-size dependent bins within the genic region (CGI, gene body, and CTCF) as to maintain the same number of bins for each feature. The average for all (I) CGI, (J) Gene Body, and (C) CTCF were assessed for each of the FCG (XXF, XXM, XYF, XYM) and plotted as averages with 95% CI. I) X-chromosome CpG Islands (CGI), shores, and shelves have higher levels of mCG in XX genotypes as compared to XY. The greatest difference in mCG is in the CGI. J) X-chromosome gene bodies and flanking regions (+/- 4 Kb) have higher levels of mCG in XX genotypes as compared to XY. The greatest difference in mCG is upstream of TSS (ie. promoter region). K) X-chromosome CTCF binding sites have higher levels of mCG in XX genotypes as compared to XY. The difference in mCG (XX-XY) is greater within the CTCF binding site than in flanking regions (+/- 4 Kb).

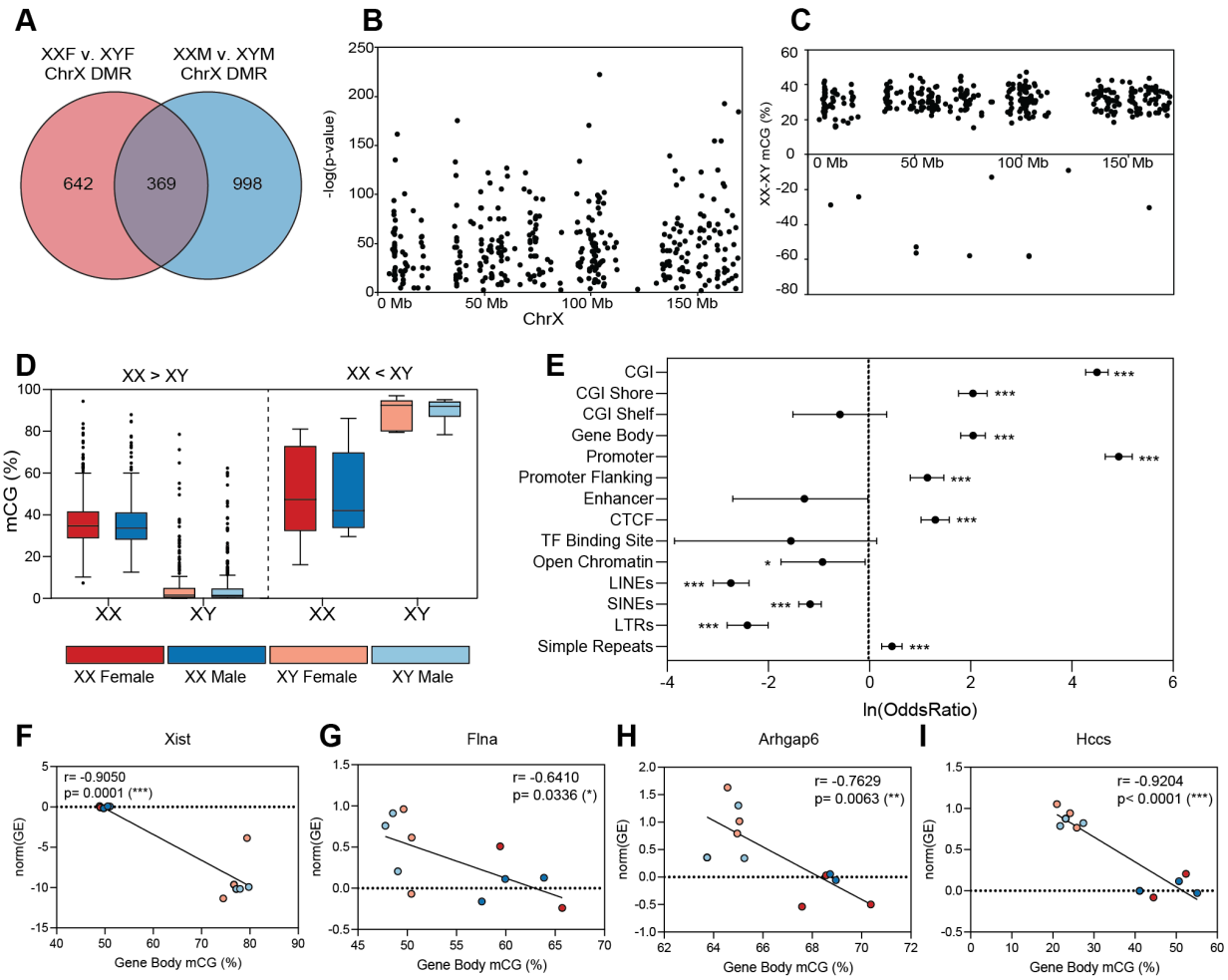

Figure 4. Epigenomic analysis of X-chromosomal differential methylation from adult FCG hippocampi. X chromosome methylation in CpG (CG) and non-CpG (CH) contexts were assessed by WGoxBS (n=3/group). Differentially methylated regions (DMRs) (w=1000) were called in methylKit. Post-hoc Student t-test with Bonferroni correction was done on pairs (XXF v. XYF, XXM v. XYM, XXF v. XXM, XYF v. XYM). A) Intersecting DMRs with significant post-hoc tests for both XX v. XY comparisons (XXF v. XYF and XXM v. XYM) identified 369 DMRs differentially methylated ChrX CpGs by sex chromosome complement. B) Significant DMRs plotted against X-chromosome coordinates show areas densely populated with DMRs and some gaps with no DMRs. C) Most (97.3%) of X-chromosome DMRs have higher mCG in XX than in XY genotypes. D) Distribution of mCG percentages for DMRs with XX > XY (left) and XX < XY (right) in FCG hippocampi. E) Comparison of X-chromosome DMRs with various genomic elements, show significant enrichment of DMRs in CGIs, CGI Shores, gene bodies, promoters, promoter flanking regions, CTCF binding sites, and simple repeats. X-chromosome DMRs were depleted in repetitive elements: LINEs, SINEs, and LTRs. F-I) Intersection of DMRs within gene bodies with differentially expressed genes by sex chromosome (XX v. XY) identified four genes: (F) *Xist,* (G) *Flna*, (H) *Arhgap6*, and (I) *Hccs*, all of which have a significant negative correlation between gene body methylation and gene expression.

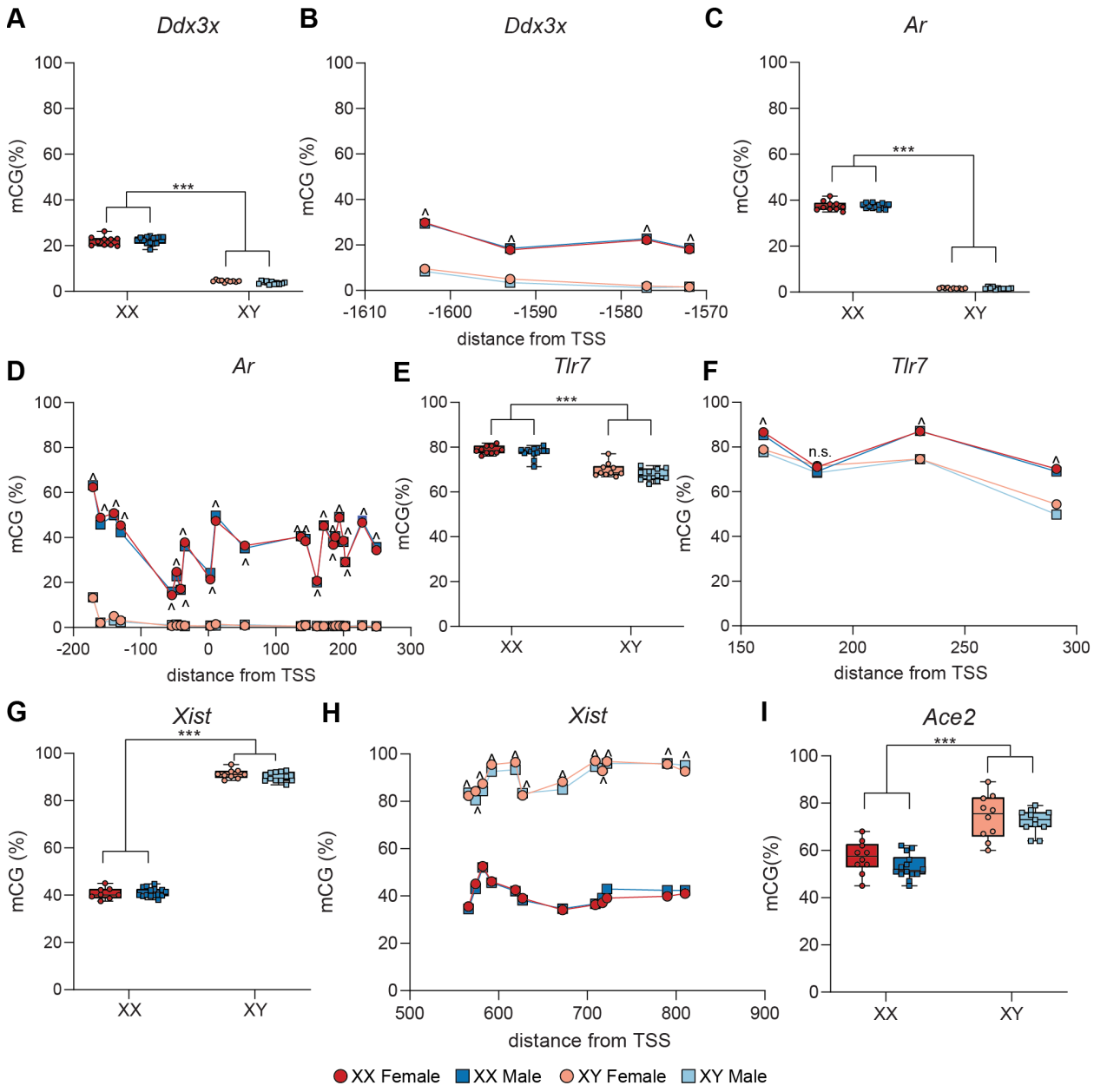

Figure 5. Targeted bisulfite amplicon sequencing (BSAS) of X-chromosome gene promoters in FCG hippocampal DNA. DNA isolated from FCG hippocampi (n=10-16/group) was bisulfite-converted and DNA methylation in gene promoters (+/- 2kb from TSS) was assessed by BSAS. (A) Average *Ddx3x* promoter mCG is lower in XY genotypes (XYF/XYM) as compared to XX genotypes (XXF/XXM), regardless of gonadal sex. (B) The topography, or patterning, of mCG across the amplified region of the *Ddx3x* promoter shows base-specific regulation of mCG by sex-chromosome complement (XX v. XY), with higher mCG in XX genotypes than XY genotypes at each CG site in the region. (C) Average *Ar* promoter mCG is lower in XY genotypes (XYF/XYM) as compared to XX genotypes (XXF/XXM), regardless of gonadal sex. (D) The topography of mCG across the amplified region of the *Ar* promoter shows base-specific regulation of mCG by sex-chromosome complement (XX v. XY), with higher mCG in XX genotypes than XY genotypes at each CG site in the region. (E) Average *Tlr7* promoter mCG is lower in XY genotypes (XYF/XYM) as compared to

XX genotypes (XXF/XXM), regardless of gonadal sex. (F) The topography of mCG across the amplified region of the *Tlr7* promoter shows base-specific regulation of mCG by sex-chromosome complement (XX v. XY), with higher mCG in XX genotypes than XY genotypes at three of the four CG sites in the region. (G) Average *Xist* promoter mCG is higher in XY genotypes (XYF/XYM) as compared to XX genotypes (XXF/XXM), regardless of gonadal sex. (H) The topography of mCG across the amplified region of the *Xist* promoter shows base-specific regulation of mCG by sex-chromosome complement (XX v. XY), with higher mCG in XY genotypes than XX genotypes at each CG site in the region. (I) Average *Ace2* promoter mCG is higher in XY genotypes (XYF/XYM) as compared to XX genotypes (XXF/XXM), regardless of gonadal sex.

Boxplots represent median, interquartile range, and minimum/maximum mCG (%) averaged over all CG sites within the amplified region of the respective gene promoter. (2way ANOVA, main effect of sex-chromosome complement (XX v. XY), ***p<0.001) (2way ANOVA, Tukey's posthoc, ^p<0.05 for all four XX v XY comparisons: XXF v XYF, XXF v. XYM, XXM v. XYM, XXM v. XYF)

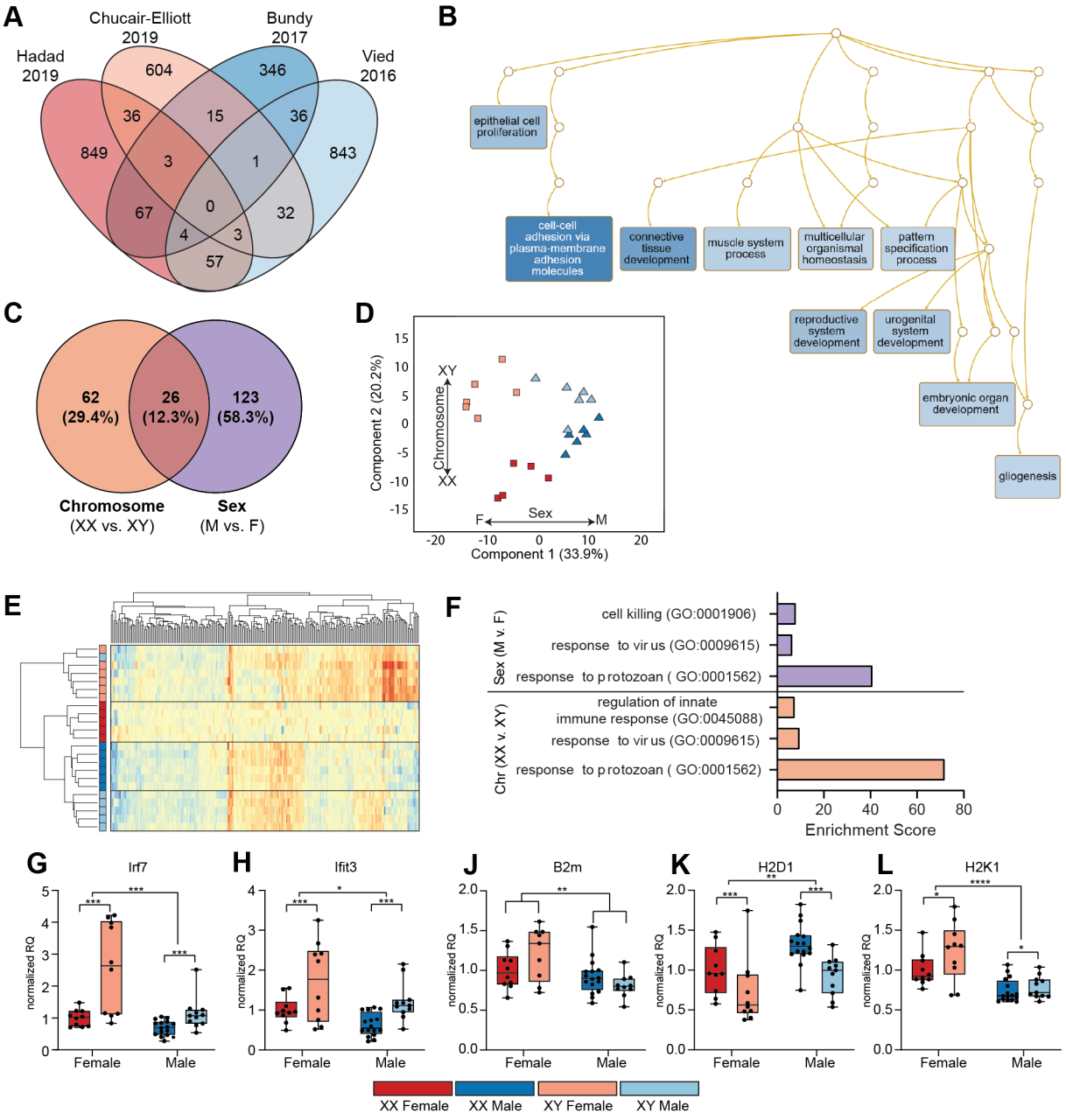

Figure 6. Transcriptomic analysis of autosomal differential expression from adult FCG hippocampi. DNA and RNA were isolated from FCG hippocampi (n=10-16/group). mRNA expression was assessed by stranded RNA-Seq (n=5-6/group) and RT-qPCR (n=10-16/group). Results were compared to previously published hippocampal transcriptomic sex differences. **Boxplots** represent median, interquartile range, and minimum/maximum normalized RQ. A) Comparison of four previous hippocampal transcriptomic studies (Supplemental Table 2), shows 2896 autosomal-encoded sex differences in wild-type mice across all studies with no genes in common between all studies. B) GO Biological Process Over-Representation Analysis (ORA) of the autosomal sex differences identified in previous studies revealed 10 major pathways differentially regulated by sex in the mouse hippocampus (Supplemental Table 3). C) Differential expression analysis of FCG hippocampal RNA-Seq libraries identified 211 differentially expressed autosomal genes, 62 had a main effect of chromosome only (XX v. XY), 123 had a main effect of sex only

(M v. F) and 26 genes had main effects of chromosome and sex. D) Principal component analysis of differentially expressed autosomal genes showed separation of sex (M v. F) in the first component (33.9%) and separation of the chromosome (XX v. XY) in the second component (20.2%). E) Hierarchical clustering of differentially expressed autosomal genes shows separation of genotypes by sex and sex chromosome complement. F) ORA of the autosomal sex differences identified in the FCG hippocampus revealed 4 pathways (Supplemental Table 3) differentially regulated by sex chromosome complement and/or gonadal sex. G-L) Differential expression of select genes was confirmed by RT-qPCR (n=10-16/group, Two-Way ANOVA, main effect of sex chromosome complement (XX v. XY) or gonadal sex (M v. F), *$p<0.05$, **$p<0.01$, and ***$p<0.001$).

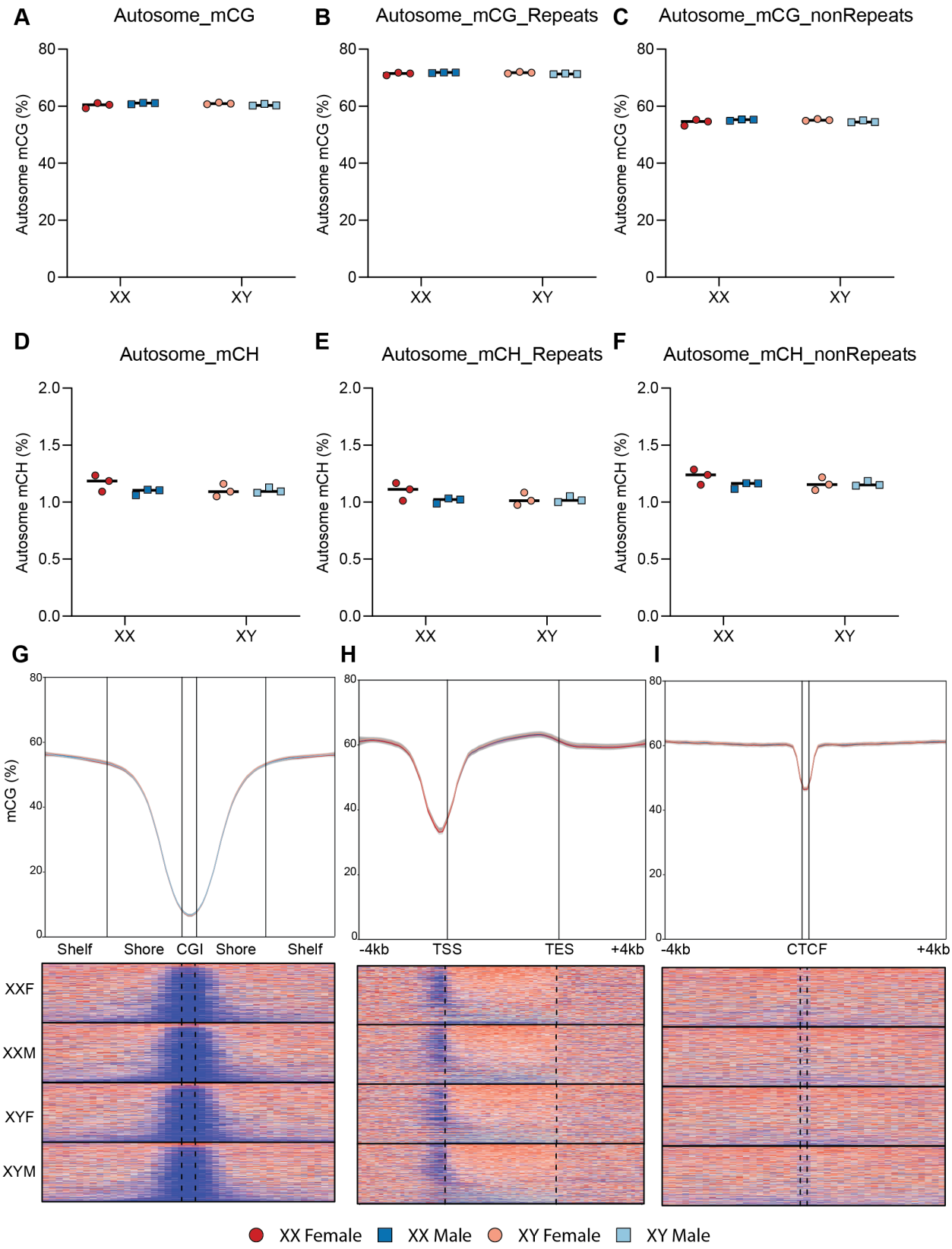

Figure 7. Autosomal chromosome levels of methylation in FCG hippocampus by WGoxBS. DNA and RNA were isolated from FCG hippocampi (n=10-16/group). Autosomal methylation in CpG (CG) and non-CpG (CH) contexts were assessed by WGoxBS (n=3/group). A) There is no difference in overall mCG on autosomes, in either (B) Repetitive or (C) Non-repetitive elements. D) There is no difference in overall mCH on autosomes in either (E) Repetitive or (F) Non-repetitive elements (Two-way ANOVA). G-I) There is no difference in autosomal mCG in: (G) CpG Islands (CGI), shores, and shelves; (H) gene bodies and flanking regions (+/- 4 Kb); or (I) CTCF binding sites and flanking regions (+/- 4 Kb).

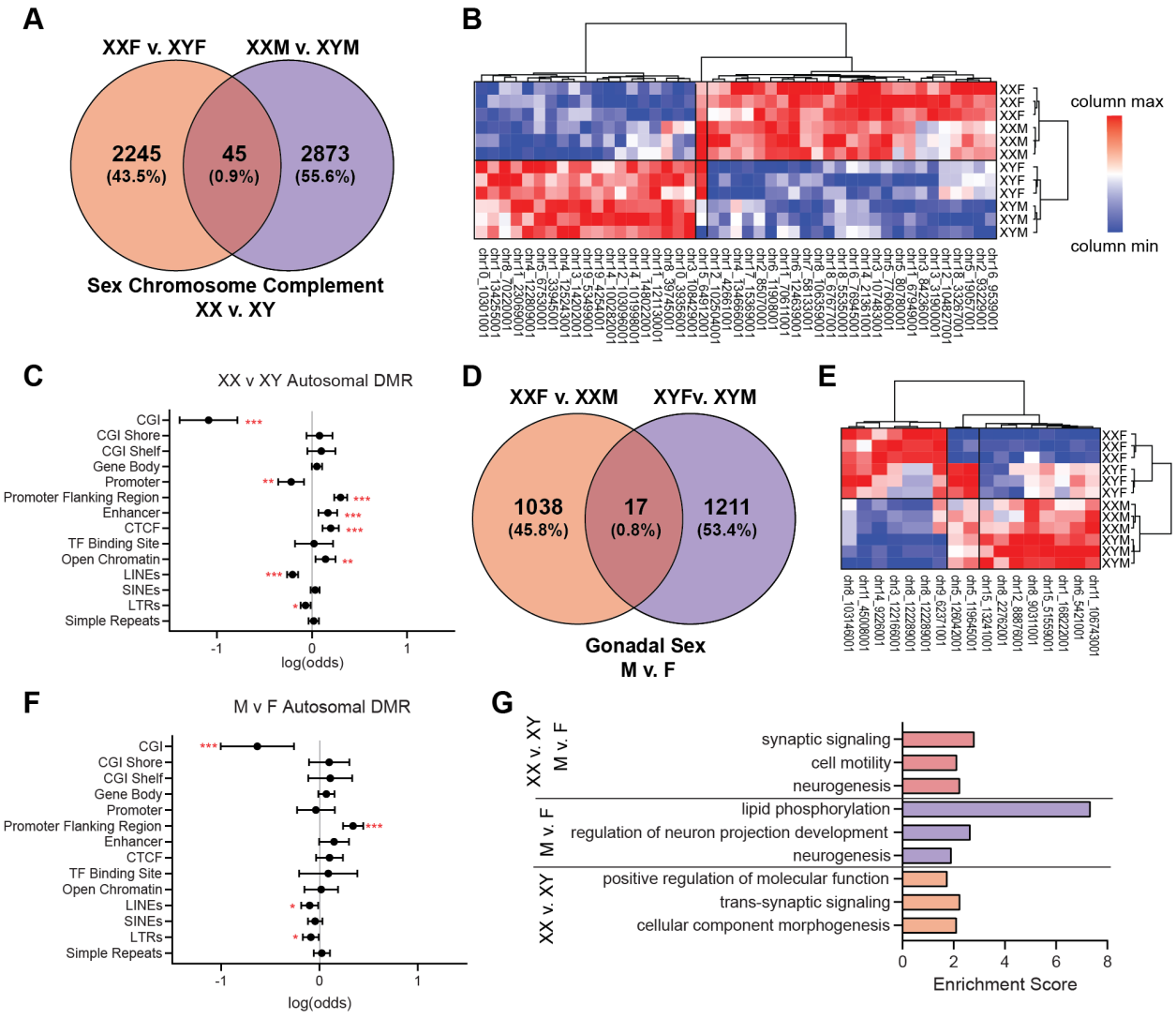

Figure 8. Epigenomic analysis of autosomal differential methylation from adult FCG hippocampi. Autosomal methylation in CpG (CG) context was assessed by WGoxBS (n=3/group). Differentially methylated regions (DMRs) (w=1000 bp) were called in methylKit. Post-hoc pairwise Student t-test with Bonferroni correction (XXF v. XYF, XXM v. XYM, XXF v. XXM, XYF v. XYM; $p < \alpha = 0.0125$). A) Intersecting significant DMRs for both XX v. XY comparisons (XXF v. XYF and XXM v. XYM) identified 47 DMRs differentially methylated autosomal CpGs by sex chromosome complement. B) Heatmap of sex chromosomally-regulated DMRs. C) Comparison of sex chromosomally regulated autosomal DMRs with various genomic elements, show significant depletion of autosomal DMRs in: CGIs, promoters, LINES, and LTRs. Sex-chromosomally regulated DMRs were enriched in: promoter flanking regions, enhancers, CTCF binding sites, and open chromatin. D) Intersecting DMRs with significant post-hoc tests for both M v. F comparisons (XXF v. XXM and XYF v. XYM) identified 17 DMRs differentially methylated by gonadal sex. E) Heatmap of gonadal sex-regulated DMRs. F) Comparison of gonadal sex-regulated autosomal DMRs with various genomic elements, show significant depletion of DMRs in: CGIs, LINES, and LTRs. Gonadal sex-regulated DMRs were enriched in: promoter flanking regions. G) Genes closest to DMRs were over-represented in GO biological process associated with neuronal functions.

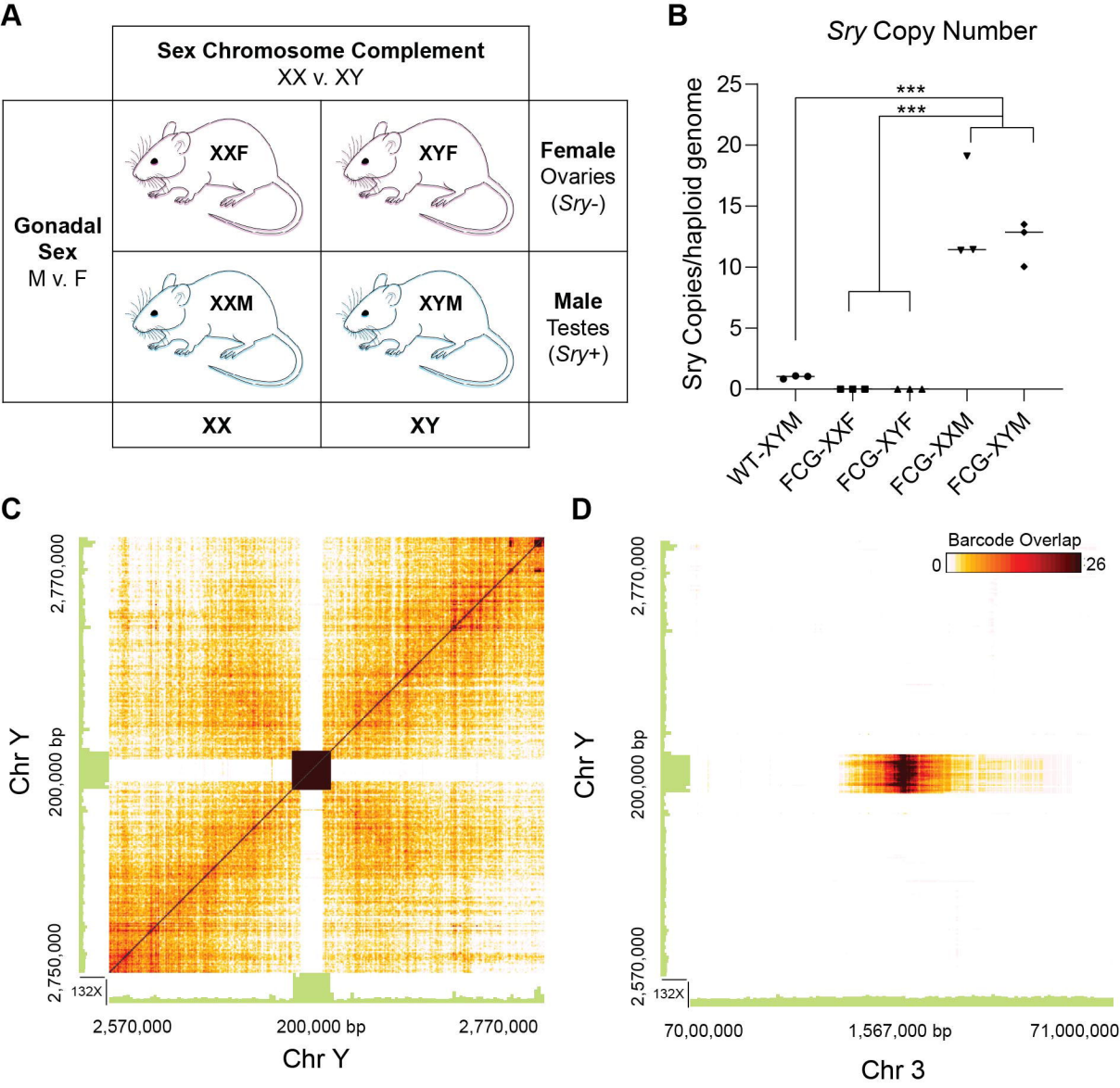
A
Sex Chromosome Complement
XX v. XY
Gonadal Sex
M v. F
XXF
XYF
XXM
XYM
Female
Ovaries
(Sry-)
Male
Testes
(Sry+)
XX
XY
B
Sry Copy Number
Sry Copies/haploid genome
25
20
15
10
5
0
***
***
WT-XYM
FCG-XXF
FCG-XYF
FCG-XXM
FCG-XYM
C
2,770,000
200,000 bp
2,750,000
Chr Y
132X
2,570,000
200,000 bp
2,770,000
Chr Y
D
Barcode Overlap
0
26
2,770,000
200,000 bp
2,570,000
Chr Y
132X
70,00,000
1,567,000 bp
71,000,000
Chr 3

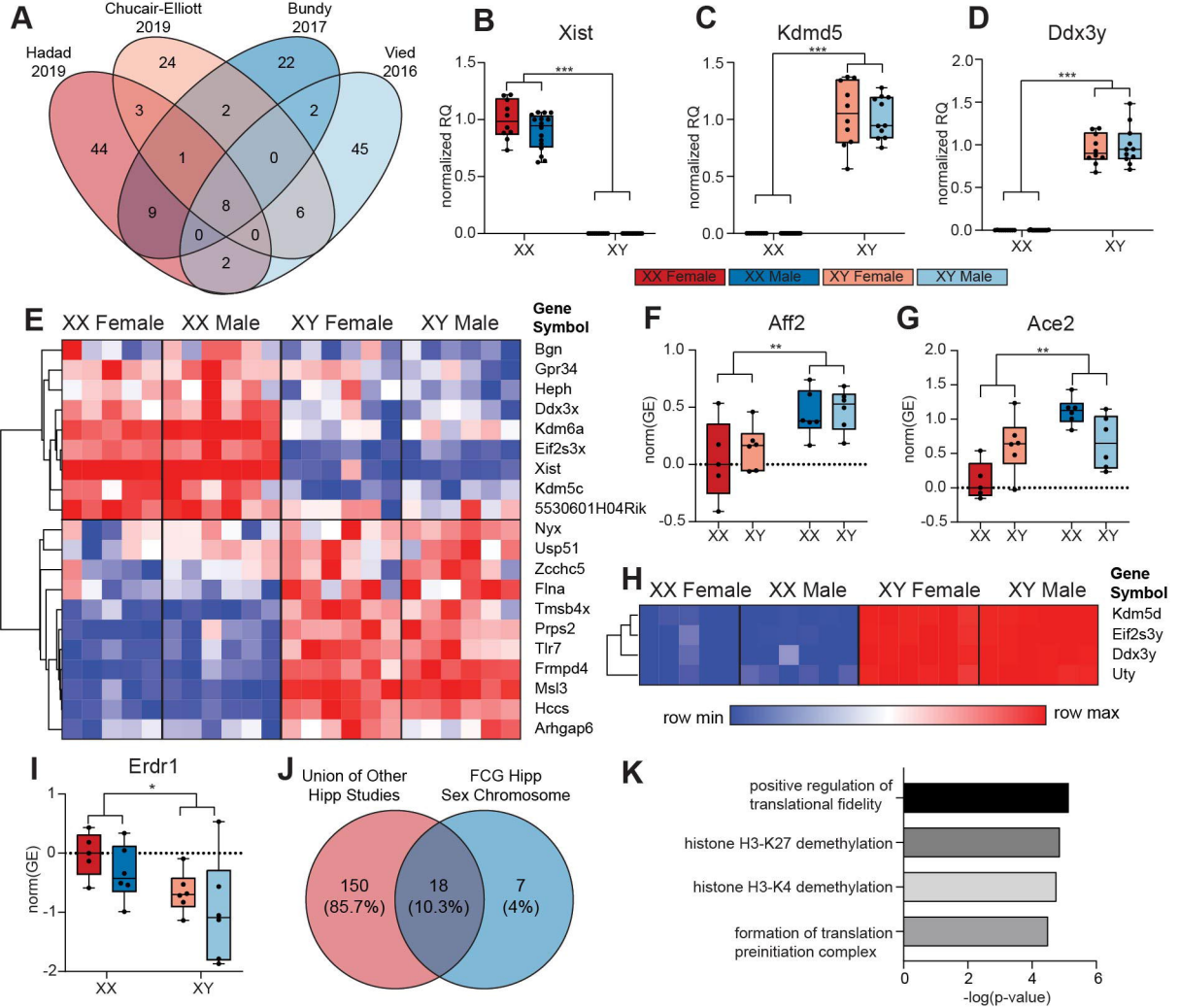
A
Chucair-Elliott 2019
Bundy 2017
Hadad 2019
Vied 2016
24
22
3
2
2
44
1
0
45
9
8
6
0
0
2
B
Xist
normalized RQ
***
XX
XY
C
Kdmd5
***
D
Ddx3y
***
XX Female
XX Male
XY Female
XY Male
E
XX Female
XX Male
XY Female
XY Male
Gene Symbol
Bgn
Gpr34
Heph
Ddx3x
Kdm6a
Eif2s3x
Xist
Kdm5c
5530601H04Rik
Nyx
Usp51
Zcchc5
Flna
Tmsb4x
Prps2
Tlr7
Frmpd4
Msl3
Hccs
Arhgap6
F
Aff2
norm(GE)
**
G
Ace2
H
Kdm5d
Eif2s3y
Ddx3y
Uty
row min
row max
I
Erdr1
*
J
Union of Other Hipp Studies
FCG Hipp Sex Chromosome
150 (85.7%)
18 (10.3%)
7 (4%)
K
positive regulation of translational fidelity
histone H3-K27 demethylation
histone H3-K4 demethylation
formation of translation preinitiation complex
-log(p-value)

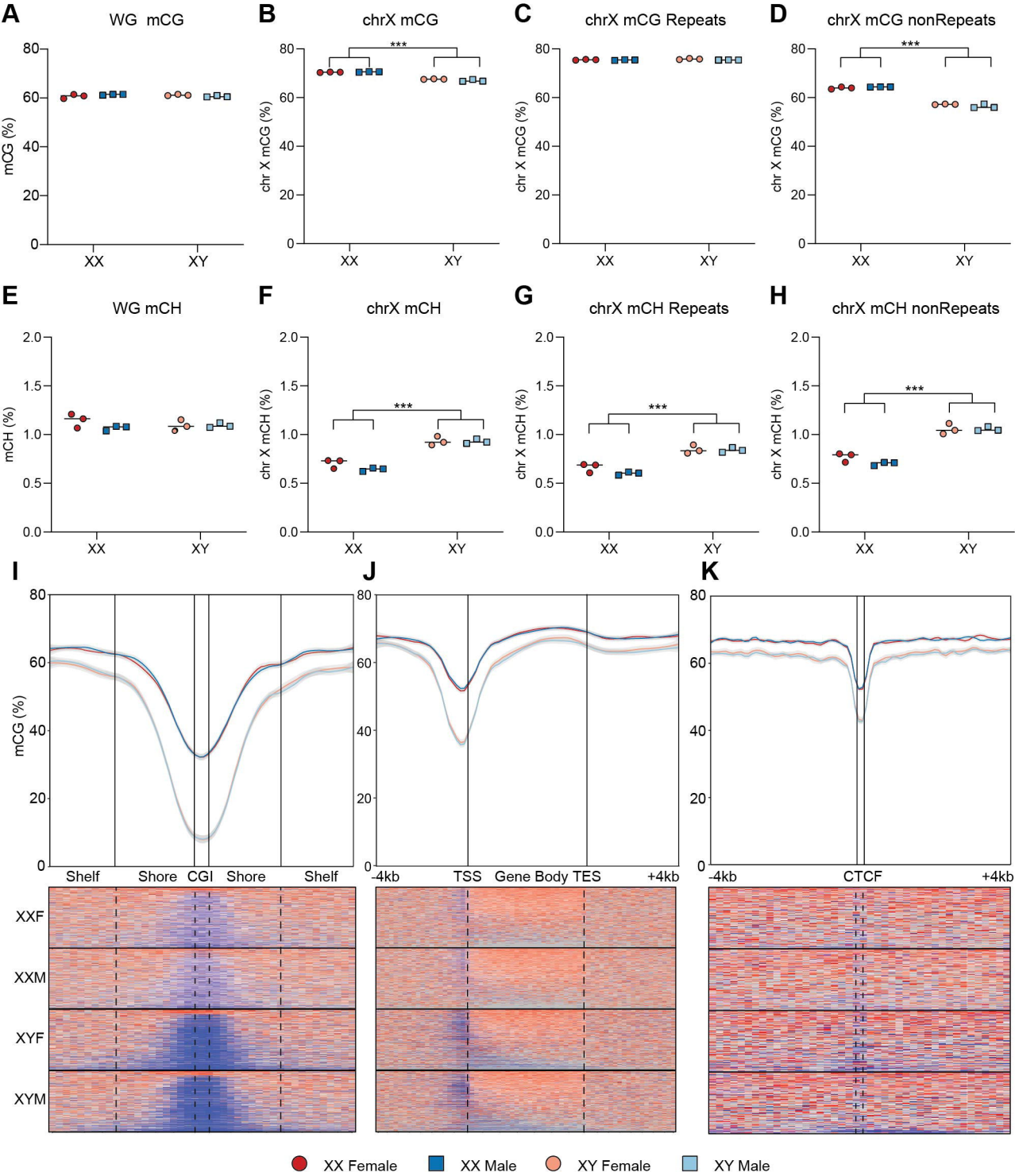
A
WG mCG
mCG (%)
B
chrX mCG
chr X mCG (%)
C
chrX mCG Repeats
chr X mCG (%)
D
chrX mCG nonRepeats
chr X mCG (%)
E
WG mCH
mCH (%)
F
chrX mCH
chr X mCH (%)
G
chrX mCH Repeats
chr X mCH (%)
H
chrX mCH nonRepeats
chr X mCH (%)
***
XX
XY
I
J
K
mCG (%)
Shelf
Shore
CGI
Shore
Shelf
-4kb
TSS
Gene Body
TES
+4kb
CTCF
XXF
XXM
XYF
XYM
XX Female
XX Male
XY Female
XY Male

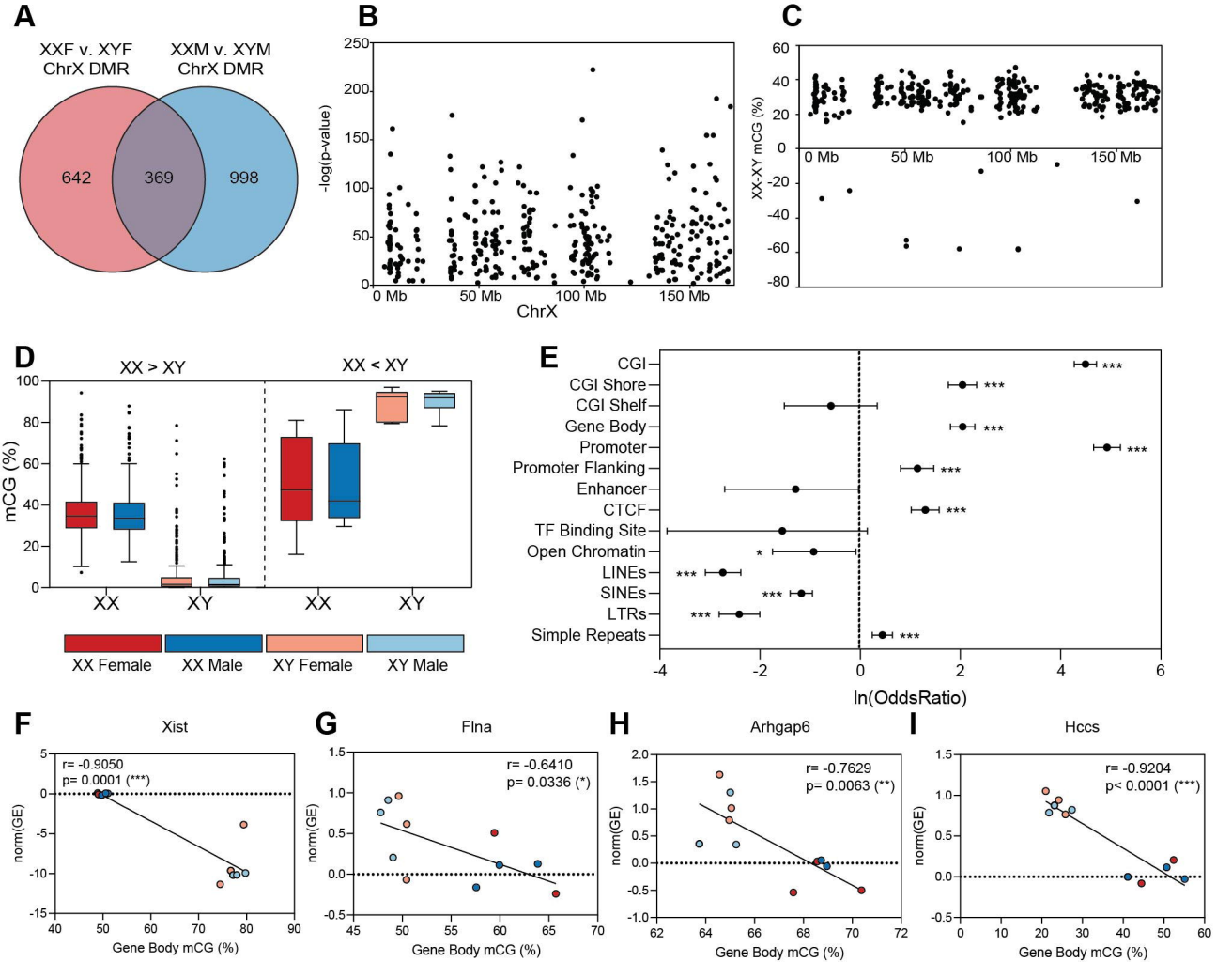
A
XXF v. XYF ChrX DMR
XXM v. XYM ChrX DMR
642
369
998
B
-log(p-value)
ChrX
0 Mb
50 Mb
100 Mb
150 Mb
C
XX-XY mCG (%)
0 Mb
50 Mb
100 Mb
150 Mb
D
XX > XY
XX < XY
mCG (%)
XX
XY
XX
XY
XX Female
XX Male
XY Female
XY Male
E
CGI
CGI Shore
CGI Shelf
Gene Body
Promoter
Promoter Flanking
Enhancer
CTCF
TF Binding Site
Open Chromatin
LINEs
SINEs
LTRs
Simple Repeats
ln(OddsRatio)
F
Xist
r= -0.9050
p= 0.0001 (***)
norm(GE)
Gene Body mCG (%)
G
Flna
r= -0.6410
p= 0.0336 (*)
norm(GE)
Gene Body mCG (%)
H
Arhgap6
r= -0.7629
p= 0.0063 (**)
norm(GE)
Gene Body mCG (%)
I
Hccs
r= -0.9204
p< 0.0001 (***)
norm(GE)
Gene Body mCG (%)

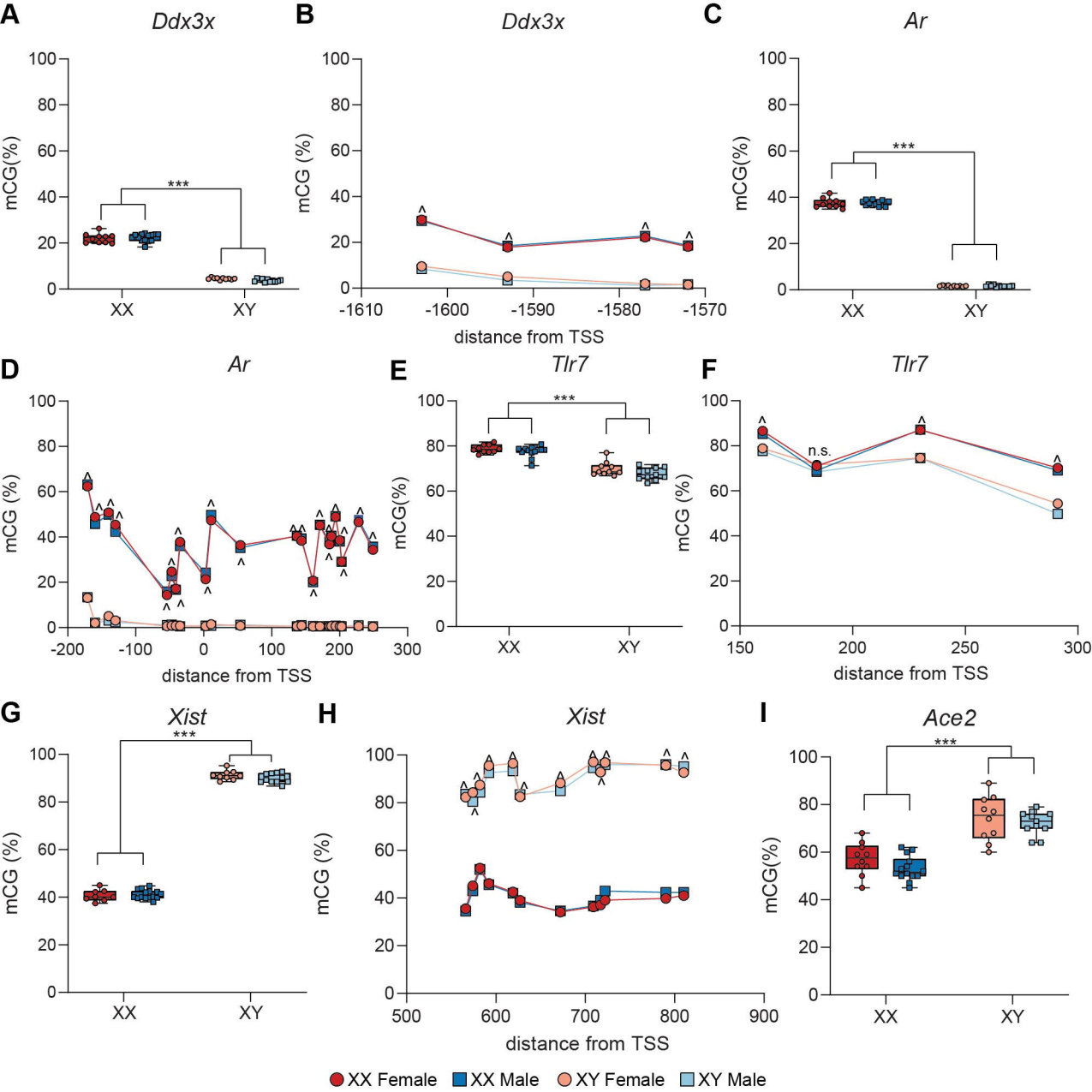
A
Ddx3x
mCG(%)
***
XX
XY
B
Ddx3x
mCG (%)
distance from TSS
C
Ar
mCG(%)
***
XX
XY
D
Ar
mCG (%)
distance from TSS
E
Tlr7
mCG(%)
***
XX
XY
F
Tlr7
mCG (%)
n.s.
distance from TSS
G
Xist
mCG (%)
***
XX
XY
H
Xist
mCG (%)
distance from TSS
I
Ace2
mCG(%)
***
XX
XY
XX Female
XX Male
XY Female
XY Male

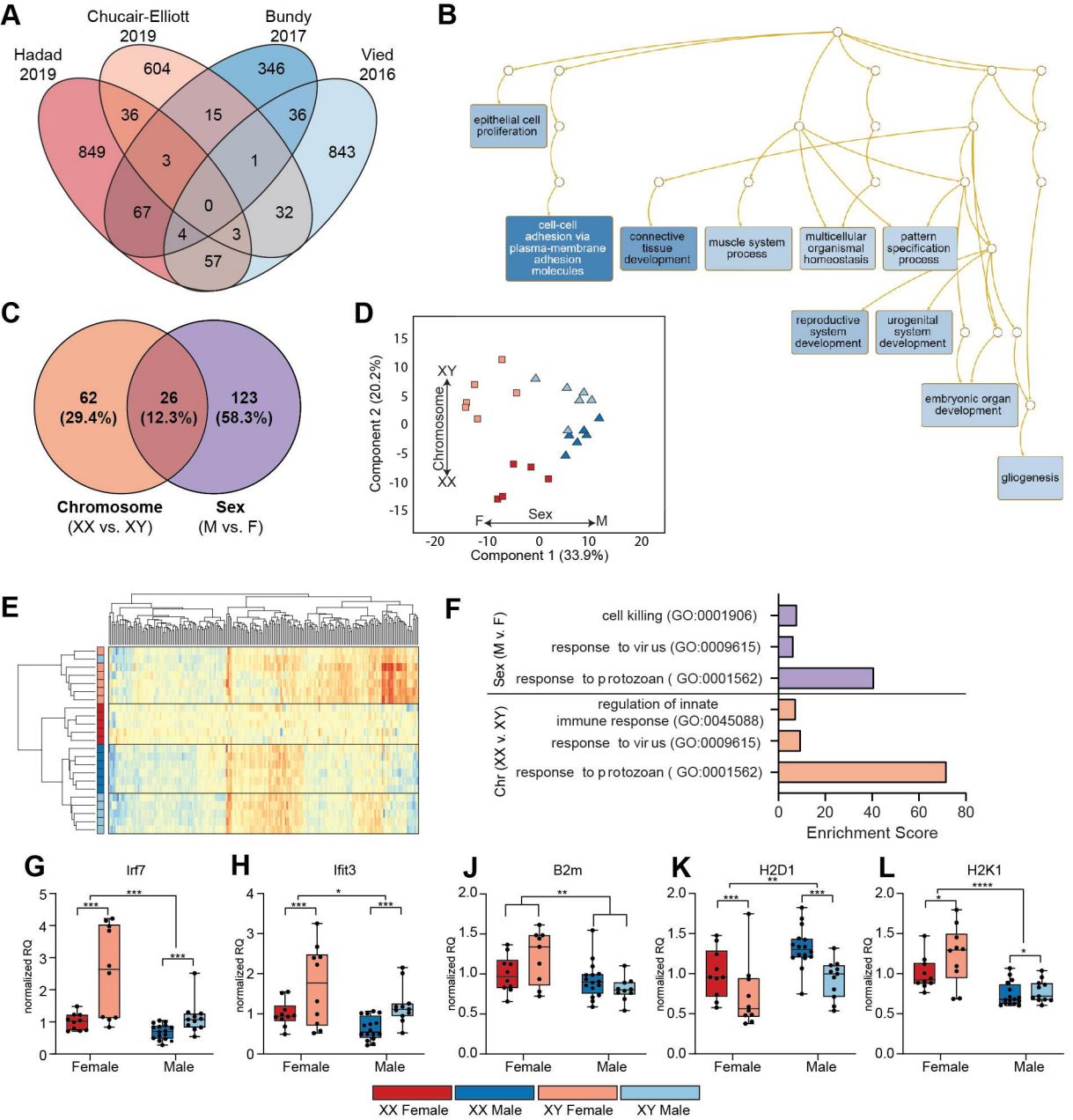
A
Chucair-Elliott 2019
Bundy 2017
Hadad 2019
Vied 2016
604
346
36
15
36
849
3
1
843
0
67
32
4
3
57
B
epithelial cell proliferation
cell-cell adhesion via plasma-membrane adhesion molecules
connective tissue development
muscle system process
multicellular organismal homeostasis
pattern specification process
reproductive system development
urogenital system development
embryonic organ development
gliogenesis
C
62 (29.4%)
26 (12.3%)
123 (58.3%)
Chromosome (XX vs. XY)
Sex (M vs. F)
D
Component 2 (20.2%)
Component 1 (33.9%)
XY
XX
Chromosome
F
M
Sex
E
F
cell killing (GO:0001906)
response to virus (GO:0009615)
response to protozoan (GO:0001562)
regulation of innate immune response (GO:0045088)
response to virus (GO:0009615)
response to protozoan (GO:0001562)
Sex (M v. F)
Chr (XX v. XY)
Enrichment Score
G
Irf7
H
Ifit3
J
B2m
K
H2D1
L
H2K1
normalized RQ
Female
Male
XX Female
XX Male
XY Female
XY Male

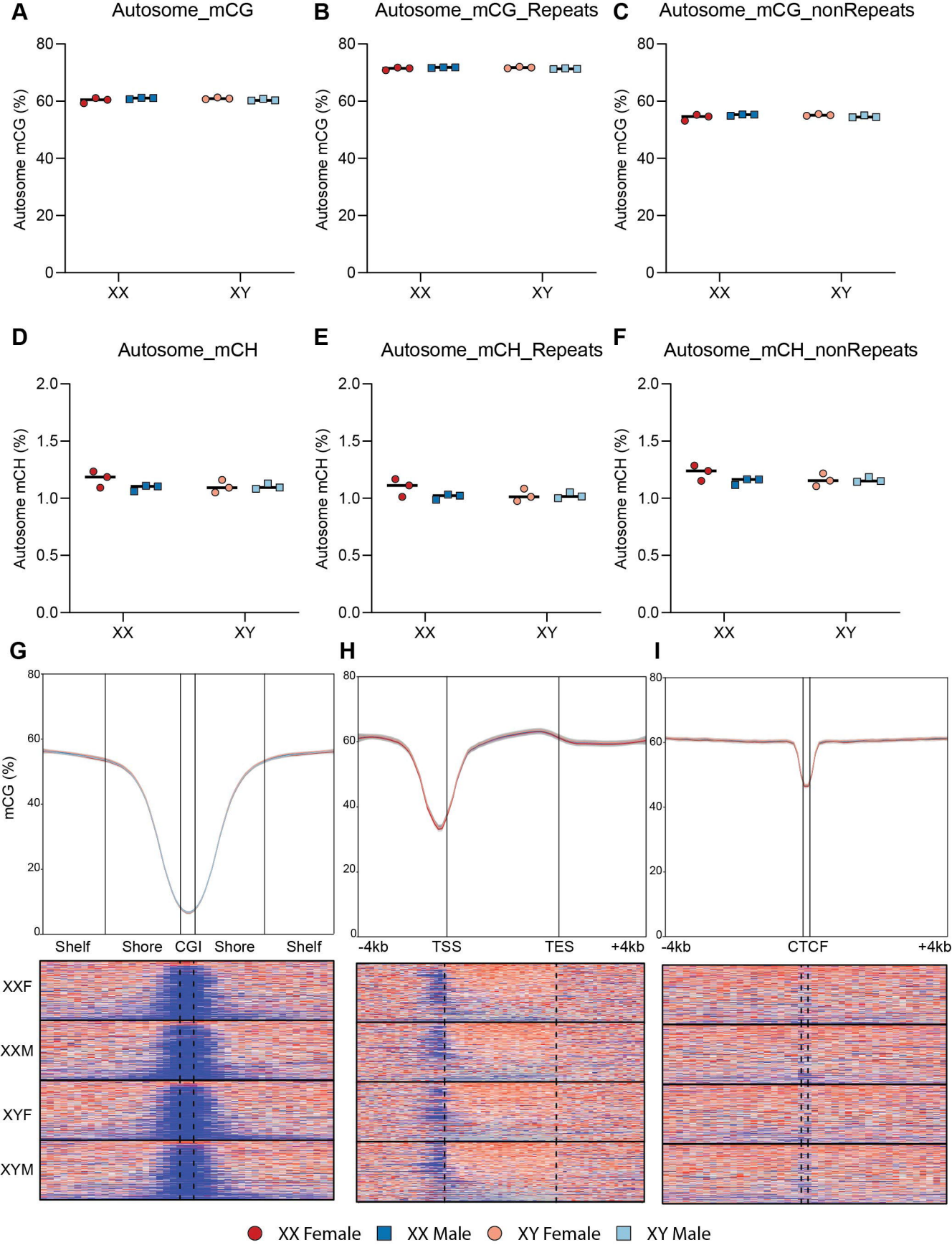
A
Autosome_mCG
Autosome mCG (%)
80
60
40
20
0
XX
XY
B
Autosome_mCG_Repeats
Autosome mCG (%)
80
60
40
20
0
XX
XY
C
Autosome_mCG_nonRepeats
Autosome mCG (%)
80
60
40
20
0
XX
XY
D
Autosome_mCH
Autosome mCH (%)
2.0
1.5
1.0
0.5
0.0
XX
XY
E
Autosome_mCH_Repeats
Autosome mCH (%)
2.0
1.5
1.0
0.5
0.0
XX
XY
F
Autosome_mCH_nonRepeats
Autosome mCH (%)
2.0
1.5
1.0
0.5
0.0
XX
XY
G
mCG (%)
80
60
40
20
0
Shelf
Shore
CGI
Shore
Shelf
H
80
60
40
20
0
-4kb
TSS
TES
+4kb
I
80
60
40
20
0
-4kb
CTCF
+4kb
XXF
XXM
XYF
XYM
XX Female
XX Male
XY Female
XY Male

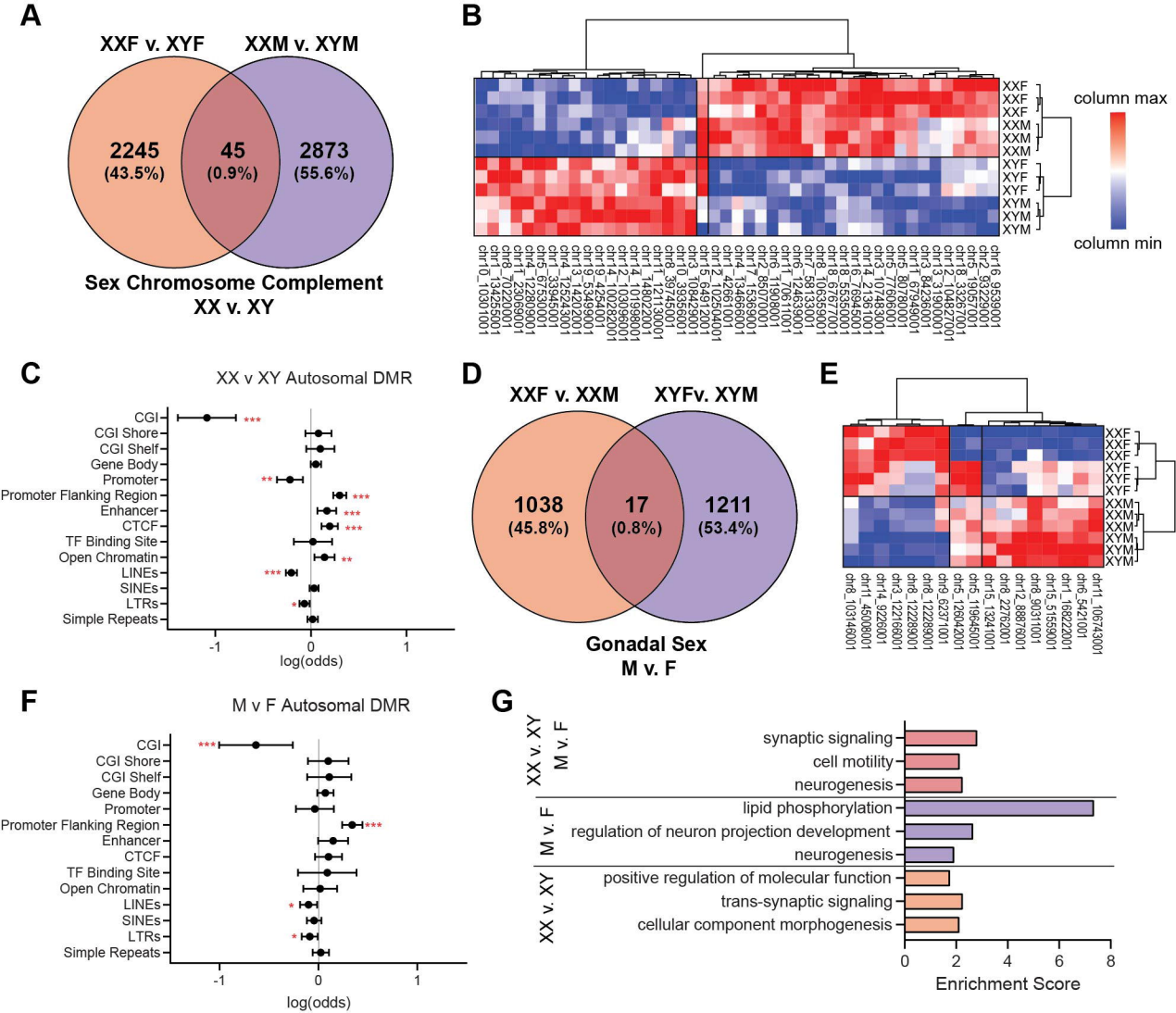
A
XXF v. XYF
XXM v. XYM
2245
(43.5%)
45
(0.9%)
2873
(55.6%)
Sex Chromosome Complement
XX v. XY
B
column max
column min
XXF
XXF
XXF
XXM
XXM
XXM
XYF
XYF
XYF
XYM
XYM
XYM
C
XX v XY Autosomal DMR
CGI
CGI Shore
CGI Shelf
Gene Body
Promoter
Promoter Flanking Region
Enhancer
CTCF
TF Binding Site
Open Chromatin
LINEs
SINEs
LTRs
Simple Repeats
log(odds)
D
XXF v. XXM
XYFv. XYM
1038
(45.8%)
17
(0.8%)
1211
(53.4%)
Gonadal Sex
M v. F
E
F
M v F Autosomal DMR
G
XX v. XY
M v. F
synaptic signaling
cell motility
neurogenesis
M v. F
lipid phosphorylation
regulation of neuron projection development
neurogenesis
XX v. XY
positive regulation of molecular function
trans-synaptic signaling
cellular component morphogenesis
Enrichment Score